Dear Dr. Marañón,

We thank the reviewer for their diligence in revising and strengthening our manuscript. Following their suggestions, we have modified the text by decreasing the emphasis on calculating export fluxes, reorganizing our discussion of the discrepancies between different productivity estimates and clarifying our conclusions. We also addressed the uncertainty in our calculations derived from the choice of respiratory quotients in the conversion of $\Delta O_2/Ar$-based calculations to molar carbon units. Finally, we have corrected typos throughout the entire manuscript. In the following, the reviewer's comments are shown in blue italicized text, with our responses below in non-italicized black text. References cited in the comments are listed in the manuscript. Please note that line numbers referenced below correspond to those in the revised manuscript that has been uploaded as a separate file. An additional version of the revised manuscript has been appended after our reviewer responses, with major revisions shown using the tracked changes function in MS Word.

However, I do think that the discussion and conclusions could be better organized and more concise. I find the discussion hard to follow at times, and I think the authors could narrow down a bit better what the most plausible processes causing the observed discrepancies are (and this should be reflected in the conclusions).

As I view it, in drifter 1, the similarities in CR but discrepancies in GPP indicate that C export alone cannot explain GPP discrepancies. Granted that there could be enhanced export during daytime, but given how similar CR rates are it would mean that the export is pretty much halted at night (actually sometimes CR-O2/Ar is larger than CR-POC). A more plausible explanation for these observations is a combination of C export and DOC dynamics. The authors mention DOC production but mostly just as a "POC loss" term, whereas the POC method is really missing a combination of DOC production and DOC respiration. If there is net DOC production during the day from newly fixed C (see Karl et al., 1998) you would expect GPP-POC to be underestimated, and respiration of fresh DOC at night (missed by the POC method) would result in an underestimation of CR-POC. If C export (that would result in an overestimation of CR-POC) is of similar magnitude than DOC respiration, CR-POC would end up being of similar magnitude than CR-O2, but differences in GPP would be greater due to DOC production. The

alternative explanation would be the proliferation of large diatoms not captured by the beam attenuation measurement, but the decrease in chla does not really support this idea.

We have condensed and reorganized our main interpretations throughout the discussion. Sect. 4.1 is now split into two rather than three sub-sections according to drifter period, and as the reviewer recommended, we have focused on the major mechanisms that could have led to discrepancies in GPP, CR and NCP over day and night intervals. Discussion of these mechanisms are described first in more detail for the drifter 1 data (Sect. 4.1.1), and again, in less detail, for drifter 2 data (Sect. 4.1.2). The decoupling mechanisms are also highlighted in our revised conclusions (lines 923-926). We removed Sect. 4.4, relocating parts of the text in other sections of the discussion and conclusions. In consolidating the discussion, we further deleted a paragraph about error in the POC mixing correction from Sect. 4.2, and instead referenced its main point in Sect. 2.7 (lines 457-460). Overall, the length of the discussion has been reduced by 36% (from 5,417 words to 3,457 words).

I do not totally understand how the correlation of 3h-NCP from both methods (Figure 5b) indicates that there are sub-daily variations in POC losses, even though I agree that potential daily changes in export could contribute to the differences. A graph showing the difference between 3-hour DeltaO2/Ar and DeltaPOC as a function of time of the day might be more useful to prove this.

We have added the plot suggested by the reviewer to Fig. 5 and referenced it in both Sect. 4.1.1 and 4.11.2 (lines 691, 753, respectively).

In drifter 2, I think that DOC dynamics alone could very well explain the differences observed. I found the discussion of the daily changes in heterotrophic biomass as a potential cause for the observed differences interesting, and I wonder whether this needs to be brought up before, with drifter 1, as it could also be affecting the differences in that case, combined with C export and DOC dynamics.

We have now moved our discussion of the effects of variable heterotrophic biomass earlier into Sect. 4.1.1 (lines 729-736) in the context of drifter site 1. We also discuss this in the context of drifter site 2, along with DOC production and carbon export (lines 774-789).

Because the authors did not measure net DOC accumulation, and the range in the reported fraction of NCP that goes into the DOC pool is quite wide, I do not think it is justifiable to estimate POC export based a chosen DOC/NCP value.

We have shortened our discussion and calculation of export fluxes, and removed all estimates of export from Sect. 4.1. Nonetheless, because we affirm the future potential for estimating export with these coupled methods, we still provide a condensed version of our export estimates just for drifter site 1 in the conclusions (Sect. 5, lines 942-945).

L479 Is a PQ of 1.1 is justifiable for NCP? If we assume that NCP approximates new production it is probably closer to 1.4.

We have assumed that drifter site 2 represents an environment with a tight microbial loop and relatively stable mixed layer, with low NO_3 concentrations and much of the photosynthetic production fueled by NH_4. Under these conditions, we feel that a PQ value of 1.1. is, indeed, appropriate (Laws 1991). We have not changed this in the revised manuscript, as it is already clarified in Sect. 2.6 (lines 311-313).

Equations: It would be helpful to specify the units of each term as well as the direction of the fluxes. I understand that tD and tN sum 1 (day), in which case (tD + tN) does not need to be added to the denominator in equations 2c and 9c. Or for consistency should be added to the denominator in equations 2a and 9a.

The terms t_D and t_N correspond to fractions of one day. On line 293, we have clarified that the dt term in the Sect. 2.6 equations has units of days (and thus rates of change are per day). We agree with the reviewer and we have added ($t_D + t_N$) to Eqs. 2 and 9 to convey that the productivity estimates are extrapolated over one full day. Additionally, we have clarified the direction of

mixing and gas exchange in lines 309-311 of the revised manuscript, and units for terms when relevant (lines 311, 345).

Eq1: shouldn't Fmix be subtracted? (positive dO2/dz means an oxygen flux into the mixed layer).

The depth gradient is calculated as deep minus surface values, and thus yields a negative term. By subtracting this negative term in equations 1 and 8, we are effectively adding it to the calculated NCP value. This has been fixed in the revised manuscript equations and in Table 1.

Eq 2b why is the PQ used to convert CR? A RQ should be used instead.

The respiratory quotients reported in past studies encompass a wider range than photosynthetic quotients (Laws 1991), from values as low as ~0.5 to as high as ~1.7 (Anderson and Sarmiento 1994; Robinson et al. 1999; Lønborg et al. 2011; Daneri et al. 2012; Fernández-Urruzola et al. 2014). Because 1.1-1.4 is a common RQ range reported in literature (Anderson and Sarmiento 1994; Robinson and Williams 1999; Robinson et al. 2002; Hedges et al. 2002), we have opted to assume that the RQ value approximates our chosen PQ for each drifter site. We have clarified this in Sect. 2.6 of the revised manuscript (lines 313-322), and describe in greater detail how this assumption may impact the results in Sect. 4.2 (lines 794-807).

Furthermore, it is not possible to apply an RQ value to several oxygen productivity terms in the manuscript, especially the mixing term, which was not differentiated between day and night. The fact that the ratio of the $\Delta O_2/Ar$ mixing term to the POC-based mixing term is roughly equivalent to the selected PQ at drifter station 1 (mean ± 1 S.D. = 1.5 ± 0.2) affirms that this conversion factor between mixing terms is reasonable.

Eq 3: The percent symbol (%) is not needed. ΔO2/Ar should be defined somewhere

In Sect. 2.2, we have defined $\Delta O2/Ar = 100\% * ([O2/Ar]_{meas} / [O_2/Ar]_{eq} - 1)$ (Tortell 2005; Tortell et al. 2011). For this reason, we do not repeat the equation in Sect. 2.6.1 and the 1/100% term is required in Eq. 3.

Eq 9a, 9b: why are these divided by the PQ? they are already in C units.

We have removed this PQ term. We thank the reviewer for catching this typo.

L780 This is a weird sentence for the results section, as the conclusions have not been presented yet.

We have removed the term "conclusions" from the sentence and rephrased it in line 628 of the revised manuscript.

L931-936 I find this paragraph confusing. Without looking at the discrepancies or similarity of GPP and CR you would be unable to know what is causing the discrepancies in NCP.

In this paragraph, we mean to convey that assumption of a constant daily respiration rate can lead to erroneous interpretations of GPP and CR. In the revised manuscript, we have moved this point to Sect. 5 as a concluding remark (lines 926-928).

Table 1. I would delete POC export estimates as the authors did not measure DOC production. Also the numbers do not seem to match my calculations.

These estimates have been deleted from the table.

Table 2. Why is the Export+DOC column only added to drifter 1?

We have filled in a similar column for drifter 2 to highlight the smaller discrepancy between NCP measures during this drifter deployment.

Decoupling of $\Delta O_2/Ar$ and particulate organic carbon dynamics in near shore surface ocean waters

Sarah Z. Rosengard[1], Robert W. Izett[1], William J. Burt[2], Nina Schuback[3], and Philippe D. Tortell[1,4]

1. Department of Earth, Ocean and Atmospheric Sciences, University of British Columbia, Vancouver, V6T 1Z4, Canada
2. College of Fisheries and Ocean Sciences, University of Alaska Fairbanks, Fairbanks, 99775, USA
3. Institute of Geological Sciences and Oeschger Center for Climate Change Research, University of Bern, Bern, Switzerland
4. Department of Botany, University of British Columbia, Vancouver, V6T 1Z4, Canada

Correspondence to: Sarah Z. Rosengard (srosengard@eoas.ubc.ca)

Abstract. We report results from two Lagrangian drifter surveys off the Oregon coast, using continuous ship-board sensors to estimate mixed layer gross primary productivity (GPP), community respiration (CR), and net community production (NCP) from variations in biological oxygen saturation ($\Delta O_2/Ar$) and optically-derived particulate organic carbon (POC). At the first drifter survey, conducted in a nearshore upwelling zone during the development of a microplankton bloom, net changes in $\Delta O_2/Ar$ and [POC] were significantly decoupled. Differences in GPP and NCP derived from $\Delta O_2/Ar$ ($NCP_{O2/Ar}$) and POC (NCP_{POC}) time series suggest the presence of large POC losses from the mixed layer. At this site, we utilized the discrepancy between $NCP_{O2/Ar}$ and NCP_{POC}, and additional constraints derived from surface water excess nitrous oxide (N_2O), to evaluate POC loss through particle export, DOC production and vertical mixing fluxes. At the second drifter survey, conducted in lower productivity, density-stratified offshore waters, we also observed offsets between $\Delta O_2/Ar$ and POC-derived GPP and CR rates. At this site, however, net [POC] and $\Delta O_2/Ar$ changes yielded closer agreement in NCP estimates, suggesting a tighter relationship between production and community respiration, and lower POC loss rates. These results provide insight into the possibilities and limitations of estimating productivity from continuous underway POC and $\Delta O_2/Ar$ data in contrasting oceanic waters. Our observations support the use of diel POC measurements to estimate NCP in lower productivity waters with limited vertical carbon export, and the potential utility of coupled O_2 and optical measurements to estimate the fate of POC in high productivity regions with significant POC export.

1 Introduction

Marine primary productivity provides the main source of organic carbon to the ocean, supporting the vast majority of marine ecosystem biomass. On short time scales, a large fraction of this fixed organic carbon is converted back to CO_2 through community respiration (CR). The difference between gross primary productivity (GPP) and CR – net community production (NCP) – sets an upper limit on the quantity of particulate organic carbon that can be exported out of the mixed layer as sinking particles, transferred to the dissolved organic carbon (DOC) pool, or consumed by upper trophic levels. Accurate assessment of NCP is thus critical to understanding trophic balance and the fate of organic carbon in the surface ocean. Traditional

incubation-based approaches to quantify GPP, net primary productivity (NPP) and CR are labor-intensive and prone to sample containment artifacts (Gieskes et al., 1979; Fogg and Calvario-Martinez, 1989; Marra, 2009; Quay et al., 2010), such that NCP remains challenging to quantify on ecologically-relevant time and space scales.

In recent years, automated *in situ* measurements of seawater optical properties have been increasingly used to estimate gross and net primary productivity from changes in optically-derived surface water POC concentrations (e.g., Graff et al., 2016; Burt et al., 2018). This approach is based on the relationship between POC concentrations and the particulate fraction of the beam attenuation coefficient (c_p) (Siegel et al., 1989; Stramska and Dickey, 1992; Gardner et al., 1993; Claustre et al., 1999; Gernez et al., 2011), which can be used to resolve diurnal variations in POC. This diurnal variability results from the daytime accumulation of photosynthetically-produced organic carbon, and nighttime loss of fixed carbon through community respiration, and can thus be used to infer NCP on daily time-scales. The accuracy of this approach depends on the key assumption that variations in c_p capture most of the variability in POC concentration, and it has been shown that beam attenuation is most sensitive to particles with a diameter range of 0.5–20 μm (Stramski and Kiefer 1991; Marra, 2002; Claustre et al., 2008). To date, most efforts to calculate daily NCP from c_p variability have focused on low productivity offshore regions, where particle sizes are small and POC losses through particle export are limited (Claustre et al., 2008; White et al., 2017). These studies have reported good agreement between optically-derived GPP estimates and independent estimates of NPP from ^{14}C incubations (White et al., 2017), suggesting a tight coupling between primary productivity and mixed layer POC dynamics over daily time scales.

Another approach to NCP quantification is based on autonomous measurements of surface water dissolved oxygen to argon ratios (O_2/Ar). Argon normalization is used to correct for any physically-induced changes in O_2 saturation, such that the derived saturation anomaly, ΔO_2/Ar, is a tracer of net biological O_2 production (Kaiser et al., 2005; Tortell, 2005; Cassar et al., 2009). At steady-state, and in the absence of significant lateral advection and vertical mixing, the sea-air flux of excess biologically-produced O_2 is equivalent to NCP. With the development of automated ship-board mass spectrometers, there has been a significant expansion of surface water O_2/Ar measurements. These data have been used to examine O_2 variability resulting from diurnal variations of photosynthesis and respiration, and to infer NCP in a variety of oceanic

ecosystems (Reuer et al., 2007; Stanley et al., 2010; Tortell et al., 2011, 2014; Hamme et al., 2012; Nicholson et al., 2015; Manning et al., 2017). Recent efforts have shown that NCP estimates from $\Delta O_2/Ar$ measurements can be corrected for vertical mixing using water column N_2O measurements as a tracer (Cassar et al. 2014; Izett et al. 2018), but application of this methodology assumes that lateral advective fluxes of O_2 are negligible.

Combined measurement of mixed layer POC and O_2 dynamics holds the potential to better constrain surface water carbon budgets in biogeochemically dynamic regions at high spatial and temporal resolution. In net autotrophic systems, an increase in $\Delta O_2/Ar$ reflects the accumulation of excess photosynthetic O_2 in the mixed layer, but provides no direct insight into the fate of the resulting organic carbon. In the absence of particle export, grazing or DOC production, an increase in $\Delta O_2/Ar$, corrected for air-sea exchange and vertical mixing, should be matched by a parallel increase in POC accumulation measured by optical sensors. By comparison, high POC export, DOC production or grazing coupled to vertical migrations would act to decouple $\Delta O_2/Ar$ from optically-derived POC measurements in the mixed layer.

Previous authors have used simultaneous O_2 and c_p measurements on moorings to describe mixed layer O_2 and POC dynamics in various marine environments (Stramska and Dickey, 1992; Kinkade et al., 1999; Dickey and Chang, 2002). However, few studies to date have compared estimates of primary productivity from simultaneous measurements on daily time scales. Briggs et al. (2018) and Alkire et al. (2012) were the first to explicitly combine concurrent measurements of O_2 and POC from *in situ* autonomous sensors to quantify mixed layer productivity during a ~2-month Lagrangian study of the 2008 North Atlantic spring bloom. Tracking daily changes in mixed layer O_2 and POC concentrations, Alkire et al. (2012) constructed a detailed budget of surface ocean organic carbon throughout the course of the bloom, using the difference between O_2-based NCP and net POC accumulation to assess the partitioning of NCP into different carbon pools (sinking particles, phytoplankton biomass, and DOC). Building on this work, Briggs et al. (2018) examined the role of respiration, particle export, and DOC production in decoupling O_2 and POC dynamics through different bloom stages, demonstrating significant differences between GPP estimates derived from O_2, beam attenuation, and backscatter measurements. To our knowledge, such a detailed examination of O_2 and POC dynamics has not been reported for other marine systems.

Here, we present new results from a field study of diel variability in $\Delta O_2/Ar$ and optical properties in two contrasting near-shore regions of the Subarctic North Pacific. Using ship-board automated sensors deployed along a Lagrangian drifter track, we resolved fine-scale temporal patterns in biological oxygen production and POC concentration in a high productivity coastal upwelling zone over the continental slope and in lower productivity stratified waters offshore. The biogeochemical differences between both sites provided a unique opportunity to compare GPP, CR and NCP estimates derived from $\Delta O_2/Ar$ and POC in contrasting trophic regimes. We expected to observe significant differences between $\Delta O_2/Ar$ and POC-derived GPP, CR, and NCP estimates in the higher productivity site, reflecting greater carbon export capacity and DOC production. By comparison, we hypothesized that discrepancies in these rates would be smaller at the lower productivity site, reflecting a tighter coupling between O_2 and POC dynamics.

The results of this investigation extend the results from the 2008 North Atlantic bloom to a high productivity coastal upwelling environment where vertical mixing fluxes significantly influence the surface water mass balance. These dynamic systems play a disproportionately important role in marine biogeochemical cycling, but they pose significant challenges for interpreting time series of ecosystem metabolism. Furthermore, our study results further expand applications of a recent field approach to correcting NCP for vertical mixing (Izett et al., 2018), suggesting that this approach has significant merit in reconstructing productivity estimates from a variety of mixed layer tracers. We discuss the implications of our coupled O_2-POC measurements for understanding biological carbon cycling in marine waters, and suggest some approaches to improve the utility of these measurements for evaluating the fate of marine primary productivity across marine trophic gradients.

2 Methods

2.1 Field site and Lagrangian surveys

Field studies were conducted on board the R/V *Oceanus* in August 2017, during a transect through the Northeast Subarctic Pacific Ocean. Two Lagrangian drifters were deployed off the Oregon coast, allowing us to track diurnal patterns in phytoplankton productivity and particulate organic carbon cycling in two distinct water masses (Fig. 1). Underway temperature

and salinity measurements, collected by a Seabird SBE 45 thermosalinograph, as well as satellite (Aqua MODIS) and ship-based chlorophyll-a (Chl-a) observations, were used to guide the specific location and timing of the drifter deployments. Drifter 1 was deployed on 20 August 2017 (~9:30 PDT), ~40 km from the Oregon coast (44.54° N, 124.58° W), in the vicinity of an upwelling feature detected based on low sea surface temperature, and elevated salinity and [Chl-a]. The drifter, consisting of a beacon, GPS transmitter and 5 m drogue, was recovered at ~18:30 on 23 August 2017 (44.40° N, 124.55° W) for a total deployment of 3 days and 9 hours. Upon recovery, the drogue was missing, implying the potential for some erratic sub-surface drifting (discussed below). Drifter 2 was deployed approximately 200 km from shore (43.75° N, 126.50 °W) in a relatively warm and low salinity water mass, with low Chl-a concentrations. This second drifter was deployed at ~07:45 on 24 August 2017, and was recovered after 2 days and six hours at ~14:00 on 26 August 2017 at 43.80° N, 126.99° W. Because the *Oceanus* lacks a dynamic positioning system, the ship was not always able to perfectly track the drifter locations. To correct for these positional offsets, we discarded any observations obtained when the ship was more than 1.5 km away from the drifter location. This filtered dataset resulted in underway measurements (Sect. 2.2) every ~15 minutes during the two drifter deployments, yielding 325 and 218 quality-controlled underway observations for drifters 1 and 2, respectively.

2.2 Underway measurements

Continuous underway measurements of surface seawater optical properties were collected using Seabird (formerly Wetlabs) ECO-BB3 and ac-s sensors, following the methods outlined in detail by Burt et al. (2018). Water was collected from the ship's seawater supply system with a nominal intake of 5 m depth. Our instrument package included fully automated data collection, and hourly filtered blanks (0.2µm), which provided measurements of dissolved seawater optical properties used to infer particulate absorption (a_p) and beam attenuation (c_p) at 82 wavelengths between 400 and ~735 nm, and backscatter (b_{bp}) at 470 nm, 532 nm, and 650 nm. The BB-3 and ac-s measurements were binned into 1-minute intervals. Prior to binning, the absorption and beam attenuation data were first sub-sampled every 50 data acquisition cycles (~12.5 seconds) to enable faster processing time. The optical measurements were accompanied by continuous surface photosynthetically active radiation (PAR) and windspeed data obtained

from a Biospherical QSR-220 PAR sensor and Gill WindObserver II ultrasonic wind sensor mounted on the ship's bow.

Chlorophyll-a (Chl-a) concentrations were derived from the particulate absorption line height at 676 nm (a_{LH}) (Roesler and Barnard, 2013). Five-minute match-ups between underway a_{LH} and discrete filtered [Chl-a] measurements from the entire cruise transect (Sect. 2.4) were used to derive a best fit coefficient for the linear relationship between a_{LH} and [Chl-a] (r^2=0.87, n= 58, p<0.01). Particulate organic carbon (POC) concentrations (µg/L) were derived from particulate beam attenuation at 660 nm ($c_{p,660}$), using the empirical model in Graff et al. (2015). Similarly, phytoplankton organic carbon (C_{ph}) concentrations were calculated, using an empirical relationship between particulate backscatter at 470 nm ($b_{bp,470}$) and [C_{ph}] in µg/L (Graff et al., 2015). We used a limited set of 5m discrete measurements (n=6; Sect. 2.4) to evaluate the relationship between POC concentrations and c_p at 660nm, and the applicability of the Graff et al. (2015) model to our observations. As shown in Fig. S1, the POC measurements were significantly correlated to c_p (r^2=0.88, p<0.05), with a slope and intercept of 391.6 ± 201.6 and 36.7 ± 79.1, respectively. This slope was not significantly different from that of the Graff et al. algorithm (419.8) although our y-intercept was higher. Notwithstanding the relatively small number of discrete POC samples, and some scatter around the regression line, the similarity of our POC-c_p calibration to that reported by Graff et al. (2015) suggests that our optically-derived POC estimates are reasonably robust.

To obtain information on the particle size spectrum, we derived the wavelength-dependent slope of particulate backscatter by fitting the three b_{bp} coefficients (470 nm, 532 nm, 650 nm) to an exponential equation (Stramska et al., 2003; Loisel et al., 2006; Kostadinov et al., 2009). Finally, to assess interference of inorganic minerals on POC, and C_{ph} variability, we calculated the wavelength-specific bulk refractive index (η_p) from backscatter/total scatter ratios ($\frac{b_{bp}}{c_p - a_p}$) and the wavelength-dependent c_p slope, following the approach of Boss et al. (2001), Twardowski et al. (2001) and Sullivan et al. (2005).

In addition to optical measurements, the seawater biological oxygen saturation anomaly ($\Delta O_2/Ar$) was measured at a ~20 second resolution using a membrane inlet mass spectrometer connected to the ship's seawater intake. The seawater ratio of dissolved O_2 and Ar was determined by diverting a continuous flow of water across a dimethylsilicone membrane interfaced with a Hiden Analytical HAL20 triple filter quadropole mass spectrometer. The O_2/Ar

ratio of air-equilibrated standards ($[O_2/Ar]_{eq}$), incubated at ambient sea surface temperature, was measured every two hours. Values of $\Delta O_2/Ar$ were thus calculated as the percent deviation of seawater O_2/Ar measurements from the air-equilibrated ratio, using $\Delta O_2/Ar = 100\% * ([O2/Ar]_{meas} / [O_2/Ar]_{eq} - 1)$ (Tortell, 2005; Tortell et al., 2011).

2.3 Mixed layer depth

Over the course of both drifter deployments, we conducted regular sampling casts (every six to ten hours) to examine depth profiles of seawater hydrography and biogeochemical variables. Temperature, salinity, dissolved O_2 concentrations and Chl-a fluorescence profile data from the CTD casts were measured by a Seabird-SBE 38 temperature sensor, Seabird-SBE 4 conductivity sensor, SBE 43 dissolved O_2 sensor, and a Seabird ECO fluorometer, respectively, and binned into 1 m intervals. Vertical profiles at the drifter 1 site showed relatively weak density stratification, likely as a result of recent upwelling. For this reason, we estimated mixed layer depths (z_{mld}) based on visible inflection points in the dissolved $[O_2]$, fluorescence and density profiles, assuming that dissolved O_2 concentrations and fluorescence are relatively uniform in the mixed layer. Within a single CTD cast, mixed layer depths varied by up to 28% across all three profile measurements. The [Chl-a] fluorescence profiles had the most well-defined inflection points, and we thus used these data to estimate z_{mld} at all casts. Excluding fluorescence profiles from the first day (Sect. 3.1), and two casts at 6am and midnight on second and third 24-hour intervals, respectively, which displayed relatively noisy density profiles, an average z_{mld} value (19 ± 2 m) was derived and applied to all subsequent analyses.

In comparison to the drifter 1 site, CTD cast profiles during drifter deployment 2 showed larger density gradients. We thus computed z_{mld} using a density difference criterion of 0.25 kg/m^3 (Thomson et al., 2003; de Boyer Montégut et al., 2004) from median values within the upper-most 4–6 m of the profile. We found that this critical density criterion was necessary to capture the depth of inflection in O_2 and [Chl-a]. In all CTD casts except one, density difference-based z_{mld} values were within 5 meters of the values derived from the inflection points on density profiles. An average z_{mld} value estimated from the density-difference approach (22 ± 5 m) was applied to all subsequent analyses.

384 **2.4 Discrete samples**

385

386 Concentrations of phosphate ([PO_4^{3-}]), dissolved silica ([SiO_2]), and nitrate and nitrite
387 ([NO_3^- + NO_2^-], were measured in seawater samples collected from daily Niskin bottle casts.
388 Following collection, nutrient samples were filtered through 0.2 µm pore polycarbonate
389 membranes and immediately frozen at -80°C on board the ship. These samples were stored at
390 -20°C until subsequent colorimetric laboratory analyses (Murphy and Riley, 1962; Riley, 1977)
391 with a Lachat QuikChem 8500 Series 2 Flow Injection Analysis System.

392 Concentrations of nitrous oxide (N_2O) were measured in discrete samples collected in
393 Niskin bottles during both drifter deployments (Fig. S2), following methods outlined in (Capelle
394 et al., 2015). These N_2O measurements were used to correct NCP estimates for vertical mixing
395 (see Sect. 2.6), following the approach described by Cassar et al. (2014) and Izett et al. (2018).
396 Profile samples from the first day of drifter deployment 1 (August 20) were omitted from
397 calculations, as underway surface temperature and salinity measurements indicated intrusion of
398 an external water mass (further discussed in Sect. 3.1) (Fig. S3). Three profiles collected from
399 12:00 (PDT) CTD casts during the following three days of the deployment (August 21, 22 and
400 23) were applied to the NCP mixing correction at drifter station 1 (Sect. 2.6.1).

401 Surface (~5 m) discrete seawater samples were collected either from Niskin bottles or
402 from the ship's surface seawater intake system for HPLC analysis of Chl-a concentrations and
403 other phytoplankton pigments. Single or duplicate samples were filtered onto 25 mm GF/F
404 filters, flash-frozen in liquid nitrogen, and stored at -80°C until analysis, following the
405 methodology described in Schuback et al. (2016). Additional samples were collected from the
406 seawater intake for size-fractionated Chl-a analysis (Zeng et al., 2018). These samples were
407 filtered through stacked 47 mm filters (0.2 µm, 2 µm and 20 µm pore size) separated by a mesh
408 spacer. Filtered samples were extracted in 5 mL of 90% acetone at 4°C until analysis within 24–
409 48 hours using a Turner Trilogy Fluorometer on board the ship.

410 Discrete samples for POC analysis were collected at two depths from several CTD casts.
411 Surface samples were collected at both drifter sites from 5 m depth, while deeper samples were
412 collected at near the base of the euphotic zone (~1% PAR), corresponding to 40–60 m at drifter
413 site 1, and 100–120 m at drifter site 2. POC samples (~1–4 L) were filtered through a pre-
414 combusted (450 °C) Whatman GF/F filter (nominal pore size ~ 0.7 µm), and stored at -80°C

until laboratory analysis. Prior to analysis, samples were thawed and dried at 50°C overnight, fumigated with concentrated hydrochloric acid for 48 hours, and dried again at 50°C overnight. POC concentrations in samples (and blank combusted filters treated as described above) were quantified using an *Elementar* vario MICRO cube CHNS analyzer. Blank-corrected discrete POC concentrations were used to validate application of the [POC] model in Graff et al. (2015) to our underway c_p data (Sect. 2.2; Fig. S1).

2.5 Net Primary Productivity

Daily-integrated net primary productivity (NPP) was calculated in two ways. First, carbon uptake was determined from 24-hour ^{14}C-incubations with 5 m triplicate seawater samples collected from early morning CTD casts. Measurements were made on two different mornings during drifter deployment 1 and on one morning during drifter deployment 2. The measurements were conducted following the protocol outlined in Hoppe et al. (2017). Depth-integrated NPP was calculated by multiplying the derived 24-hour volumetric carbon fixation rate by the average mixed layer depth for the respective drifter period.

Second, daily-integrated net primary productivity was also estimated as a product of $[C_{ph}]$ values derived from b_{bp}, and phytoplankton growth rates according to the carbon-based production model (CbPM) (Behrenfeld et al., 2005; Westberry et al., 2008; Graff et al., 2016; Burt et al., 2018). In these calculations, daily-averaged $[C_{ph}]$, $[Chl\text{-}a]/[C_{ph}]$, and mixed layer irradiance (E_g) calculated from the MODIS-derived surface PAR matched to drifter location were used to calculate growth rates and NPP every 24 hours. Chlorophyll-a concentrations were derived from absorption line height, $[C_{ph}]$ values from b_{bp} (Sect. 2.2), and light extinction coefficients (K_d) obtained from [Chl-a] to calculate E_g (Morel et al., 2007). An average mixed layer depth for each drifter period was applied to estimate mixed layer NPP (Sect. 2.3).

2.6 Quantification of GPP, CR and NCP

Gross primary productivity (GPP), community respiration (CR) and net community production (NCP) rates were calculated based on linear regressions of $\Delta O_2/Ar$ and POC against time (dt in units of days) over subsequent day (D) and night (N) intervals during both drifter

deployments. Daytime was defined as the period during which PAR levels exceeded 20 µmol quanta $m^{-2}s^{-1}$. The average length of the day-time period was 13.6 ± 0.14 hours over the two drifter deployments. In the following sections, t_d represents the day length normalized to 24 hours, and t_n analogously represents the fractional night length, equivalent to 1-t_d. All daily rates were integrated through the mixed layer using the average z_{mld} for each drifter period, as described in Sect. 2.3.

2.6.1 O_2/Ar-derived rates

Quantification of $GPP_{O2/Ar}$, $CR_{O2/Ar}$, and $NCP_{O2/Ar}$ rates from diurnal cycles in ΔO_2/Ar (Ferrón et al., 2015) requires corrections for gas exchange and, potentially, vertical mixing fluxes. For these calculations, we first computed the rate of change in ΔO_2/Ar (dO_{2Bio}/dt) using linear regression analysis within successive day or night intervals. We then derived estimates for the air-sea gas exchange (J_{ex}) and vertical mixing fluxes (F_{mix}) over the respective time interval to isolate the NCP contribution to observed ΔO_2/Ar changes (Izett et al., 2018; Tortell et al., 2014). A negative J_{ex} indicates net transfer of O_2 from the atmosphere to the mixed layer, while a negative F_{mix} indicates vertical transfer of ΔO_2/Ar-depleted to the mixed layer, both in units of mmol m^{-2} d^{-1}. Gross O_2 production rates were converted into carbon units using a photosynthetic quotient (PQ) for new production of 1.4 for drifter period 1 calculations and a PQ for regenerated production of 1.1 for drifter period 2 (Laws, 1991). Community respiration rates were converted into carbon units using the same PQ values, and considered constant over each respective day length period (i.e., $t_d + t_N$). This assumption of an equivalent respiratory quotient (RQ) and PQ within each drifter period is reasonable given the wide range of respiration ratios reported in prior studies across a range of oceanic environments (Anderson and Sarmiento, 1994; Robinson and Williams, 1999; Robinson et al., 1999; Hedges et al., 2002; Robinson et al., 2002; Lønborg et al., 2011; Daneri et al., 2012; Fernández-Urruzola et al., 2014). Moreover, Robinson and Williams (1999) estimated lower RQ values at lower productivity stations in the Arabian Sea, suggesting that it is reasonable to assume a lower RQ value (equivalent to PQ= 1.1) at drifter site 2.

$$NCP_{\frac{O2}{Ar},D\ or\ N} = z_{mld}\left.\frac{dO_{2bio}}{dt}\right|_{D\ or\ N} + J_{ex}|_{D\ or\ N} - F_{mix} \quad (1)$$

$$GPP_{O2/Ar} = \frac{t_d(NCP_{\frac{O2}{Ar},D} - NCP_{\frac{O2}{Ar},N})}{PQ(t_d+t_N)} \quad (2a)$$

$$CR_{O2/Ar} = \frac{NCP_{\frac{O2}{Ar},N}}{PQ(t_d+t_N)} \quad (2b)$$

$$NCP_{\frac{O2}{Ar},24hr} = \frac{t_d NCP_{\frac{O2}{Ar},D} + t_N NCP_{\frac{O2}{Ar},N}}{PQ(t_d+t_N)} \quad (2c)$$

$$O_{2bio} = \Delta\frac{O_2}{Ar}\frac{1}{100\%}O_{2eq} \quad (3)$$

$$J_{ex} = k_{o2}O_{2bio} \quad (4)$$

$$F_{mix,O2/Ar} = k_{mix}\frac{dO_{2bio}}{dz} = k_{N2O}N_2O_{bio}\frac{dO_{2bio}}{dN2O_{bio}} \quad (5)$$

$$k_{mix} = k_{N2O}N_2O_{bio}\left(\frac{dN2O_{bio}}{dz}\right)^{-1} \quad (6)$$

$$N_2O_{bio} = N_2O_{meas} - N_2O_{eq} - N_2O_{thermal} \quad (7)$$

Equilibrium concentrations of O_2 and N_2O ($[O_2]_{eq}$ and $[N_2O]_{eq}$) were calculated using the salinity and temperature-dependent equations of Garcia and Gordon (1992) and Weiss and Price (1980), respectively, and sea surface temperature and salinity from the ship's thermosalinograph. Estimates of surface excess N_2O saturation, $[N_2O]_{bio}$, included a heat flux correction to account for solubility changes (Keeling and Shertz, 1992; Jin et al., 2007; Izett et al., 2018). Non-weighted piston velocities (k_{O2} and k_{N2O}; units of m d^{-1}) were calculated using the diffusive air sea gas flux and Schmidt number parameterizations of Wanninkhof (2014) and Raymond et al. (2012), and ship-based wind speed data 10 m above the sea surface. Daytime and nighttime estimates for the gas exchange term, J_{ex}, were calculated using day/night average $[O_2]_{eq}$, $\Delta O_2/Ar$, and k_{O2} values. Vertical gas gradients ($\frac{dN2O_{bio}}{dz}$ and $\frac{dO_{2bio}}{dN2O_{bio}}$) were estimated from our discrete

N_2O measurements and Rosette O_2 profiles over the upper 100 m of the water column, following Izett et al. (2018).

At drifter site 1, daily F_{mix} values were calculated using daily $[N_2O]_{bio}$, daily vertical gradient and daily average k_{N2O} values, and converted to carbon units using a PQ of 1.4. Denitrification should not have been a source of N_2O within the upper 100 m of the water column because measured O_2 concentrations were consistently greater than the threshold value of ~50 mmol m^{-3} (e.g., Hopkinson and Barbeau, 2007). Likewise, we assumed no lateral advection of N_2O into drifter site 1, as there were little differences in the mixing ratio $[O_2]_{bio}/[N_2O]_{bio}$ across profile measurements (Fig. S2). While the August 22 CTD cast did exhibit a more anomalous $[O_2]_{bio}/[N_2O]_{bio}$ profile relative to the other two cast profiles, inclusion of these data had little impact on the vertical mixing correction. At drifter site 2, we assumed that vertical mixing was negligible due to the presence of strong density stratification, and therefore did not calculate a mixing flux correction at this site. In any case, the presence of a sub-surface O_2 maximum (Fig. S2) at this site would limit the application of the N_2O correction (Izett et al., 2018).

2.6.2 Optically-derived rates

We used the approach of Claustre et al. (2008) and White et al. (2017) to calculate daily-integrated GPP_{POC}, CR_{POC}, and NCP_{POC} from daytime and nighttime changes in POC (dPOC/dt), derived from linear regressions of POC concentrations against time through day and night intervals. In certain ocean environments, NCP_{POC} will not equate to $NCP_{O2/Ar}$ as a result of additional POC sinks, including export, grazing and DOC production. Under these conditions, CR_{POC} includes these loss terms, and therefore NCP_{POC} more accurately reflects net POC accumulation, as will be discussed further in Sect. 4. Nonetheless, for consistency with previous studies, we use the term NCP_{POC} to describe the quantities computed in Eq. 8.

$$NCP_{POC,D\ or\ N} = z_{mld} \left.\frac{dPOC}{dt}\right|_{D\ or\ N} - F_{mix(POC)} \quad (8)$$

$$GPP_{POC} = \frac{t_d(NCP_{POC,D} - NCP_{POC,N})}{t_d + t_N} \quad (9a)$$

$$CR_{POC} = \frac{NCP_{POC,N}}{t_d + t_N} \quad (9b)$$

$$NCP_{POC,24hr} = \frac{t_d NCP_{POC,D} + t_N NCP_{POC,N}}{t_d + t_N} \quad (9c)$$

The presence of significant upwelling at drifter site 1 provides additional complexity in the estimate of NCP from optically-derived POC measurements. In particular, vertical transport of particle-deficient seawater from below the mixed layer into the surface could dilute the c_p signal used to derive POC concentrations (Stramska and Dickey, 1994). To address this, we applied the vertical mixing term, k_{mix}, derived from Eq. (6) to estimate the average daily dilution effect on mixed layer POC concentrations through drifter period 1:

$$F_{mix,POC} = k_{mix} \frac{dPOC}{dz} \quad (10)$$

A negative $F_{mix,POC}$ indicates transfer of [POC]-deficient seawater into the mixed layer. The term d[POC]/dz represents the vertical gradient in [POC], derived from daily average POC concentrations measured in Rosette samples at 5 m and near the base of the euphotic zone, below the mixed layer (40–60 m) (Sect. 2.4). The dz term was calculated as the difference between the average mixed layer depth from all CTD casts and the daily average shallowest depth of minimum particle concentrations based on beam transmission profiles. At drifter site 2, $F_{mix,POC}$ was considered negligible (Sect. 2.6.1) due to the high density stratification of the water column.

In total, three sets of 24-hour GPP, CR and NCP values were calculated during the drifter 1 deployment from the three pairs of consecutive day and night intervals, starting with the first night interval and ending with the last day interval. We excluded the first day-time interval from our calculations, due to the erratic salinity values observed during the first day of this drifter deployment (Sect. 3.1; Fig. S3). Because the drifter period was terminated prior to sunset, the last day interval was 1.6 hours shorter than the average daytime duration. For the second drifter deployment, two sets of GPP, R and NCP values were calculated from consecutive day and night intervals, starting with the first daytime interval and ending with the last nighttime interval. The initiation of the drifter period occurred after sunrise, so the first day interval was 1.1 hours shorter than the average daytime duration.

562 **2.6.3 Integration time scales**

563

564 The approach to calculating NCP on the basis of linear regressions utilizes the high
565 temporal resolution of our data set. We compared our results from Sects. 2.6.1 and 2.6.2 to NCP
566 values calculated using several of other integration time scales. Following studies that have
567 calculated daily NCP values from "instantaneous" rates of change (e.g., hourly rates in Hamme
568 et al. (2012) and Tortell et al. (2014)), we divided our NCP calculations into shorter increments.
569 Given that the average measurement interval was ~15 minutes (after removing values where the
570 ship was not sufficiently close to the drifter; Sect. 2.1), we calculated NCP within three-hour
571 intervals:

572

573 $$NCP_{\frac{O_2}{Ar},3hr} = \frac{3}{24}\left[z_{mld}\left(\frac{dO_{2bio}}{dt}\right)_{3hr} + J_{ex,3hr}\right]/PQ \quad (11a)$$

574 $$NCP_{POC,3hr} = z_{mld}\left[\frac{3}{24}\left(\frac{dPOC}{dt}\right)_{3hr}\right] \quad (11b)$$

575

576 For each day of the drifter periods, eight consecutive three-hour NCP values were summed into a
577 24-hour period to yield daily NCP estimates. We then applied the vertical mixing correction to
578 these daily estimates (refer to Eqs. 5, 6, 10), since the correction was only available on a daily
579 basis given the lower sampling resolution of [N_2O] and [POC] profiles. We also calculated daily
580 NCP using the difference between ΔO_2/Ar or [POC] between two time points at the beginning
581 and end of each 24-hour period (similar to the approach in Alkire et al. (2012); and Barnes and
582 Antoine (2104)). Finally, we calculated a single daily NCP rate per drifter period using the linear
583 regression of ΔO_2/Ar and [POC] against time over the entire drifter deployment. For these latter
584 two approaches, the 24-hour average and drifter-period average of relevant terms in Eqs. 1-9
585 were used to calculate NCP, and a PQ was used to convert O_2 to carbon units.

586

587 **2.7 Error analysis**

588

589 Errors for all estimates of net primary productivity (CbPM-NPP, ^{14}C-NPP) and net
590 community production ($NCP_{O2/Ar}$, NCP_{POC}) were propagated from uncertainties associated with
591 all variables used for the computations. Error estimates for time-averaged variables were

generally represented by the standard deviation, as we assumed that this significantly exceeded the error of the individual measurements prior to averaging. The uncertainty in z_{mld}, derived from the standard deviation of mixed layer depths across individual CTD casts, was 2 m for drifter site 1 and 5 m for drifter site 2 (Sect. 2.3). Small uncertainties in t_D and t_N were calculated as the standard deviations of all day or night lengths measured during both drifter periods (0.14 and 0.10 hours, respectively). Mean relative errors of [Chl-a] and [C_{ph}] from Burt et al. (2018), and mean relative standard deviations in MODIS-derived daily surface PAR values were propagated to calculate the error in CbPM-NPP. The standard deviations of triplicate 24-hour ^{14}C uptake incubations were propagated to calculate the error in ^{14}C-NPP estimates. The uncertainties in ^{14}C-NPP values are likely underestimated, as they do not account for bottle effects, as discussed in Sect. 4.3.

For calculating error in NCP, uncertainties in dO_{2bio}/dt and dPOC/dt were derived from the confidence interval of the best-fit slope of linear regression of each variable against time. Standard deviations of averaged $\Delta O_2/Ar$, k_{O2}, and k_{N2O} values, and the mean relative errors of $[N_2O]_{meas}$, $[N_2O]_{Eq}$, $[N_2O]_{thermal}$, and $\frac{dO_{2bio}}{dN2O_{bio}}$ reported in Izett et al. (2018), were propagated into the mixing correction errors for $NCP_{O2/Ar}$ and NCP_{POC}. The error in $\frac{dN2O_{bio}}{dz}$ was calculated as the confidence interval of the best fit slope extracted from a linear regression of pooled drifter 1 $[N_2O]_{bio}$ values against depth. In propagating the error associated with the dPOC/dz term in Eq. 10, we have included the standard deviation of the minimum transmissivity depth across daily CTD casts and the standard deviation of POC measured in multiple blank combusted filters (Sect. 2.4). Finally, to account for variability in the PQ and RQ, we assumed an uncertainty of 0.1, following the range reported Laws (1991).

3 Results

3.1 Water mass properties

Ship-board underway measurements revealed clear differences in hydrographic and biogeochemical characteristics between the water masses sampled by the two drifters. Surface water properties at drifter site 1 reflected the presence of a recently upwelled water mass that was

622 relatively cold (11.8 ± 0.4 °C), saline (32.6 ± 0.04 g/kg), and nutrient-rich (Figs. 1, S3, S4). The
623 Pacific Fisheries Environmental Laboratory's coastal upwelling index at 45°N, 125°W was
624 positive throughout drifter period 1. In contrast, the water mass tracked by the second drifter
625 deployment was warmer (17.5 ± 0.1°C) and fresher (31.8 ± 0.05 g/kg), with lower average mixed
626 layer nutrient concentrations.
627 Examination of surface water hydrographic properties during the two drifter deployments
628 suggest that both drifters tracked a relatively homogenous water mass, excluding a period of
629 salinity variability during the first day of drifter deployment 1, and several transient temperature
630 and salinity excursions after the second night of this deployment (grey patches in Fig. S3). These
631 features indicate potential intrusion of external water masses, possibly a result of loss of the
632 drifter drogue (Sect. 2.1). Observations during these periods were thus removed from the data set
633 prior to analysis. Outside of these intervals, variability in salinity (drifter 1: 32.5–32.7 g/kg;
634 drifter 2: 31.8–31.9 g/kg) was small during both drifter deployments. Variability in sea surface
635 temperature was also limited (drifter 1: 11.2–13.0 °C, drifter 2: 17.3–17.7 °C), and largely
636 reflected a diurnal variation of warming and cooling, which was particularly evident for drifter
637 period 2.
638 Temporal differences in CTD cast profiles point to some variation in mixed layer depth
639 (z_{mld}) during both drifter deployments. In general, there were no multi-day trends or regular
640 diurnal patterns in z_{mld} through both periods, suggesting that transient shifts in water column
641 turbulence likely contributed to changes in the shape of temperature, salinity, dissolved oxygen
642 and fluorescence profiles. Average z_{mld} values, calculated over each drifter period, had relatively
643 low relative standard deviations (<25%) and were applied to all subsequent calculations (Sect.
644 2.3). A sensitivity analysis, not shown, indicated that the choice of mixed layer depth using
645 different criteria (i.e., fluorescence profiles, density profiles and the density difference criterion)
646 and different time scales of integration (i.e., daytime/nighttime, 24 hour, and multi-day) did not
647 significantly impact the results discussed below.
648 Average mixed layer nutrient concentrations fluctuated during both drifter deployments,
649 but did not exhibit regular diurnal cycles (Fig. S4). At drifter site 1, concentrations ranged from
650 0.74 to 0.85 µM phosphate, 7.8 to 9.0 µM nitrate and nitrite, and 9.2 to 11.1 µM dissolved silica,
651 excluding day 1 of the drifter deployment and anomalously high concentrations measured during
652 a noisy CTD cast at midnight on the last day of the deployment. Excluding these outliers, a

significant ($p<0.05$) linear regression of each nutrient concentration against time revealed that phosphate concentrations decreased by ~0.07 µM, [NO_3^- + NO_2^-] decreased by 0.9 µM, and [SiO_2] decreased by 1.2 µM over the three-day drifter period, roughly in Redfield ratio proportions (Sect. 3.4). Nutrient concentrations varied less at site 2, from 0.08–0.10 µM [PO_4^{3-}], 0.29–0.61 µM [NO_3^- + NO_2^-], and 1.2–1.7 [SiO_2]. While [PO_4^{3-}] and [SiO_2] increased significantly ($p<0.05$) by 0.015 µM and 0.48 µM, respectively, these changes were small compared to the nutrient drawdown observed during drifter period 1, and did not reflect Redfield ratio proportions. It is possible that intrusions of an external water mass with slightly elevated nutrient concentrations contributed to the small increase in [PO_4^{3-}] and [SiO_2] measured during these CTD casts, even though we assume that such effects on our derived productivity estimates are negligible based on inspection of underway temperature and salinity data (Fig. S3).

3.2 Biogeochemical comparisons between drifter sites

Elevated nutrient concentrations at the drifter 1 site supported high productivity and the accumulation of phytoplankton biomass, as indicated by elevated chlorophyll-a ([Chl-a]= 0.66–1.5 µg/L), phytoplankton carbon ([C_{ph}]= 83–115 µg/L) and particulate organic carbon concentrations ([POC]= 130–261 µg/L) (Figs. 2a–c). We observed [C_{ph}]/[Chl-a] ratios ranging from 68–143 g/g, with a median value of 85 g/g (Fig. 2f). Using the carbon-based production model (CbPM; Sect. 2.5) and daily-averaged mixed layer PAR derived from satellite values matched to drifter location (within 5 km), these [C_{ph}]/[Chl-a] ratios translate into phytoplankton growth rates ranging from 0.75–0.94 d^{-1}. At the second drifter site, phytoplankton productivity and biomass were significantly lower in the nutrient-poor waters ([Chl-a]= 0.06–0.21 µg/L, [C_{ph}]= 11–17 µg/L, and [POC]= 25–38 µg/L). Ratios of [C_{ph}] to [Chl-a] at site 2 were significantly higher ($p<0.05$) than those observed at site 1, ranging from 69 g/g to 203 g/g, with a median value of 108 g/g. The higher ratios may reflect reduced cellular [Chl-a] associated with greater nutrient limitation, higher daily-integrated PAR, and proportionally more picoplankton than microplankton at drifter site 2 (Westberry et al., 2008; Hirata et al., 2011; Graff et al., 2016; Burt et al., 2018). Median PAR levels were higher and less variable at site 2, in part contributing to lower variability in CbPM-based growth rates, which ranged from 0.81 to 0.85 d^{-1}.

Several lines of evidence suggest that the phytoplankton assemblage at drifter site 1 was enriched in large-celled phytoplankton, as compared to drifter site 2. The wavelength-dependent slope of particulate backscatter (b_{bp}) was lower at site 1 (range: 1.4 to 1.6, median: 1.5) than at site 2 (range: 1.9–2.3, median: 2.1) (Fig. 2d), suggesting proportionally larger particle sizes (Stramska et al., 2003; Kostadinov et al., 2009). This observation is supported by size-fractionated Chl-a measurements. During the drifter 1 deployment, the >20 μm size fraction (Sect. 2.4), increased from 21 % to 46 % of the total Chl-a pool, indicating the enrichment of large phytoplankton in the assemblage. Pigment-based estimates of phytoplankton taxonomic composition and size class (Hirata et al., 2011; Zeng et al., 2018) suggested that relative diatom and microplankton abundances exceeded 50% on the final sampling time point. By comparison, size-fractionated [Chl-a] and HPLC analyses from drifter 2 indicated a lower proportion of large-celled phytoplankton, with 9–15% of total [Chl-a] in the >20 μm size fraction, and diatoms and micro-plankton estimated to account for 19–29% of the phytoplankton assemblage. The proportion of picoplankton increased through time at drifter site 2 from 31–50% of total [Chl-a], alongside a slight increase in b_{bp} slope, indicating accumulation of smaller particle sizes (Fig. S3d). Finally, median bulk refractive index values across three wavelengths (470 nm, 532 nm, 650 nm) were higher at site 1 (1.08–1.11) than at site 2 (1.02–1.04) (Fig. S3e), which is consistent with a greater proportion of diatom-derived silica in the particle pool (Lide, 1997; Twardowski et al., 2001).

3.3 Diurnal variability and primary production

As shown in Fig. 3a, clear diurnal cycles in biological oxygen saturation ($\Delta O_2/Ar$) were observed during both drifter deployments. Generally, values of $\Delta O_2/Ar$ increased from dawn to dusk and decreased from dusk to dawn, yielding positive slopes of linear regressions of $\Delta O_2/Ar$ against time in the daytime, and negative slopes at night. During drifter deployment 1, this diurnal cycle was superimposed on a longer-term increase in biological O_2 saturation as under-saturated values returned toward atmospheric equilibrium. At least part of this increase is attributable to gas exchange, which would act to erase O_2 under-saturation in the mixed layer caused by recent upwelling. However, calculation of the sea-air O_2 flux shows that, except for the first 24-hour period, only a small amount of the daily increase in $\Delta O_2/Ar$ can be explained by

714 gas exchange (absolute value of J_{ex} < 10 mmol O_2 m^{-2} d^{-1}) (Table 1). Thus, the temporal change
715 in $\Delta O_2/Ar$ can be attributed to a primarily biological source. The magnitude of this increase is
716 further underestimated because of vertical upwelling of deep oxygen-poor waters, which would
717 act to dampen the increase in $\Delta O_2/Ar$ through time. After accounting for a mixing correction
718 ranging between 22 and 97 mmol m^{-2} d^{-1} O_2 (equivalent to 16 to 70 mmol m^{-2} d^{-1} C when
719 assuming a photosynthetic quotient of 1.4), daily-integrated gross primary productivity
720 ($GPP_{O2/Ar}$) ranged from 270 to 358 mmol C m^{-2} d^{-1}, and community respiration ($CR_{O2/Ar}$) rates
721 ranged from 74 to 172 mmol C m^{-2} d^{-1} (Table 1).
722 Examination of the diel variability in POC and Chl-a during drifter period 1 revealed
723 significant differences in the behavior of these variables as compared to $\Delta O_2/Ar$ (Fig. 3b, c). In
724 particular, while $\Delta O_2/Ar$ increased during the first drifter deployment, [POC] and [Chl-a] values
725 decreased. We estimated that vertical mixing ($F_{mix,POC}$), accounted for 12 to 68 mmol m^{-2} d^{-1} C of
726 these daily changes in [POC], similar to the magnitude of the mixing correction for $\Delta O_2/Ar$
727 variability (Table 1). After taking mixing into account, daily-integrated GPP_{POC} decreased from
728 242 mmol m^{-2} d^{-1} on day 1 to 98 mmol m^{-2} d^{-1} on day 3, while CR_{POC} rates ranged from 77 to
729 147 mmol m^{-2} d^{-1}.
730 Calculated daily averaged net primary productivity (NPP) were lower than $GPP_{O2/Ar}$.
731 Rates derived from the CbPM model (Sect. 2.5), declined from 147 mmol C m^{-2} d^{-1} on day 1 of
732 drifter deployment 1 to 112 mmol C m^{-2} d^{-1} on day 3 (Table 1), reflecting the trend in Chl-a
733 concentrations used to derive NPP (Fig. 3c). The CbPM-derived NPP estimates were similar to
734 that obtained in ^{14}C incubations (150 ± 18 mmol C-$m^{-2}d^{-1}$) within the first 24 hours of drifter
735 deployment 1. However, ^{14}C-based NPP estimates on the third day of the deployment (49 ± 8
736 mmol C-$m^{-2}d^{-1}$) were about two-fold lower than those obtained from CbPM calculations.
737 Dissolved oxygen and POC dynamics at drifter site 2 differed significantly from those
738 observed at site 1. Compared to the drifter site 1, diel variability in $\Delta O_2/Ar$ and [POC] was more
739 tightly coupled during the second drifter deployment (Fig. 3a, b). Both O_2/Ar and [POC]
740 displayed regular diurnal variations, increasing in the daytime to a maximum around dusk and
741 decreasing at night to a minimum around dawn. Over the full drifter deployment, concentrations
742 of Chl-a and, to a lesser extent, POC, decreased, in contrast to $\Delta O_2/Ar$, which remained relatively
743 constant across days. Daily-integrated $GPP_{O2/Ar}$ values ranged from 108 to 219 mmol C m^{-2} d^{-1}
744 and $CR_{O2/Ar}$ rates ranged from 82 to 186 m^{-2} d^{-1}. POC-derived values were considerably lower

and less variable, from 41 to 38 for GPP_{POC} and 36 to 44 for CR_{POC} (Table 1). NPP derived from CbPM calculations was 22 mmol C m^{-2} d^{-1} on the first day of the drifter period and 18 mmol C m^{-2} d^{-1} on the second day, while NPP calculated from one ^{14}C bottle incubation during the first day of the drifter 2 deployment was 12 ± 4 mmol C m^{-2} d^{-1}, showing good agreement with the CbPM calculations.

3.4 Net community production

Daily net community production (NCP) rates were calculated using linear regressions of $\Delta O_2/Ar$ and POC over day and night intervals, corrected for gas exchange and vertical mixing (Sect. 2.6.1, 2.6.2). During drifter period 1, $NCP_{O2/Ar}$ and NCP_{POC} exhibited contrasting trends, as $NCP_{O2/Ar}$ remained >100 mmol C m^{-2} d^{-1} throughout, while NCP_{POC} declined to negative values on the second and third days (Table 1; Fig. 4). The transition to negative NCP_{POC} values over the course of the drifter 1 deployment primarily reflected diminishing daytime rates of POC accumulation (dPOC/dt term in Eq. 8). At drifter period 2, we observed closer agreement between NCP values. $\Delta O_2/Ar$-derived NCP ranged from -12 to 33 mmol C m^{-2} d^{-1} over two consecutive 24 hour periods, while NCP_{POC} values ranged from -3 to 1 mmol C m^{-2} d^{-1}. These lower rates at drifter site 2 are consistent with the lower observed phytoplankton biomass and nutrient concentrations.

Additional constraints on NCP during drifter period 1 can be derived from examining nutrient drawdown. Because vertical upwelling of nutrient-replete waters would dampen the magnitude of observed nutrient drawdown over time (Sect. 3.1; Fig. S4), we used the derived k_{mix} from Eq. 6 and a best-fit vertical gradient in nutrient concentrations between the mixed layer and 100 m (Sect. 2.4) to account for this mixing flux. This correction increases the cumulative three-day nutrient drawdown by 2.1 to 2.6 times. Over the three-day drifter deployment, surface Si, N and P concentrations declined in a ratio of 17: 13: 1, which is consistent with the stoichiometry expected for organic matter produced by a diatom-rich assemblage (Brzezinski et al., 1998; Turner et al., 1998; Brzezinski, 2004). Assuming that the observed decrease in SiO_2 concentrations over the three days is attributable to growth of diatoms in the mixed layer, and applying a stoichiometric ratio of 106 C: 16 Si, we estimate an average C production rate of ~128 mmol C m^{-2} d^{-1} for the drifter period. This value is consistent with $NCP_{O2/Ar}$ rates, which

were 137 mmol C m^{-2} d^{-1} on average over three days, but significantly greater than NCP_{POC} estimates (7 mmol C m^{-2} d^{-1} on average) (Table 2).

Table 2 summarizes comparisons among NCP values calculated using day/night linear regressions of $\Delta O_2/Ar$ and POC against time, and other approaches described in Sect. 2.6.3. In general, the different calculation methods did not significantly alter the results. NCP values derived from one linear regression over each drifter period agreed well with the average of two (drifter 2) to three (drifter 1) daily NCP values calculated via the other approaches. Small differences between linear regression-based NCP values and both NCP calculated from either 3-hour increments or two time points are likely due to the effect of lower signal to noise in $\Delta O_2/Ar$, $[O_2]_{bio}$ and [POC] values utilized in these latter two approaches. The following discussion thus focuses on productivity rates derived from day/night linear regressions (i.e., Eqs. 1 and 8), which utilize all data points while minimizing uncertainty in the derived rates of change. The exception is the $NCP_{O2/Ar}$ value calculated for day 1 of drifter period 2 using the daytime/nighttime linear regression method. By this approach, we calculated $NCP_{O2/Ar}$ as 26 mmol C m^{-2} d^{-1}, even though the time series in Fig. 3a clearly indicates a net decrease in $\Delta O_2/Ar$ over the 24-hour period, and all other $\Delta O_2/Ar$-based NCP calculations (Sect. 2.6.3) yielded negative values. For the discussion, Table 1 and Fig. 4, the NCP value derived from the integrated 3-hour increments represents net community production during this particular interval.

Deleted: our main conclusions were not significantly altered by

4 Discussion

A number of previous studies have examined diurnal variation in upper ocean phytoplankton and organic particle dynamics across a variety of productivity regimes, from oligotrophic environments (Claustre et al., 1999, 2008; Wu et al., 2010; Gernez et al., 2011; Kheireddine and Antoine, 2014; Thyssen et al., 2014; Nicholson et al., 2015; Ribalet et al., 2015; White et al., 2017), to higher productivity waters and phytoplankton blooms (Brunet and Lizon, 2003; Wu et al., 2010; Gernez et al., 2011; Alkire et al., 2012; Dugenne et al., 2014; Kheireddine and Antoine, 2014; Needham and Fuhrman, 2016; Briggs et al., 2018). In general, these studies have shown that more productive environments exhibit higher amplitude diurnal variations in beam attenuation, POC concentration, phytoplankton cell abundances, Chl-a, and metabolic rates. These prior results are consistent with the differences we observed between the two

distinct Northeast Pacific trophic environments represented by drifter sites 1 and 2, respectively (Sect. 3.2; Fig. 2).

Biogeochemical properties during the first Lagrangian survey suggested a dynamic, highly productive phytoplankton community, influenced by upwelling and elevated mixed layer nutrient concentrations (Figs. 1, S4). Several lines of evidence imply the presence of a developing diatom bloom at this site (Sect. 3.2; Figs. 2, 3). Increasing mixed layer biological oxygen saturation ($\Delta O_2/Ar$) was contrasted by a general decrease in particulate organic carbon (POC) concentrations, suggesting a significant decoupling between O_2 and POC dynamics. This was reflected in significant differences between $\Delta O_2/Ar$-derived gross primary productivity (GPP) and net community production (NCP) rates derived from $\Delta O_2/Ar$ and POC measurements (Figs. 4, 5; Table 1). In contrast, biogeochemical properties during the second drifter deployment were indicative of a lower productivity, nutrient-limited phytoplankton assemblage, with near-zero $\Delta O_2/Ar$ values reflecting a close balance between water column photosynthesis and respiration (Fig. 3a). Relative to the drifter 1 site, diurnal variations in $\Delta O_2/Ar$ and POC were more closely coupled, while phytoplankton biomass (C_{ph}) and chlorophyll-a (Chl-a) concentrations (dominated by smaller cells) varied little through time. Contrary to our expectations, even though $NCP_{O2/Ar}$ and NCP_{POC} rates agreed well, we also observed significant discrepancies between $GPP_{O2/Ar}$ and GPP_{POC} and between $CR_{O2/Ar}$ and CR_{POC} during drifter period 2. The contrasting properties between the two drifter deployments enable us to examine the coupling of O_2 and POC dynamics under different ecological states, with implications for the use of $\Delta O_2/Ar$ and POC measurements as proxies for GPP and NCP.

4.1 Decoupling of O_2 and POC dynamics in the mixed layer

4.1.1. Drifter 1. In the absence of significant POC sinking and net loss to the dissolved organic carbon (DOC) pool, POC-based productivity rates should approximate $\Delta O_2/Ar$-based rates (Claustre et al., 2008; White et al., 2017). However, at drifter station 1, both $GPP_{O2/Ar}$ and $NCP_{O2/Ar}$ greatly exceeded GPP_{POC} and NCP_{POC}, respectively (Figs. 4, 5a; Table 1). Over the three successive 24-hour periods of drifter deployment 1, the absolute difference between GPP measures increased from 41 mmol C m^{-2} d^{-1} to 260 mmol C m^{-2} d^{-1}, while the absolute difference between NCP estimates increased from 42 mmol C m^{-2} d^{-1} to 193 mmol C m^{-2} d^{-1}. This

Commented [MOU1]: Moved from Sect. 4.4

Deleted: The results from our Lagrangian surveys illustrate diurnal dynamics in two contrasting productivity regimes off the Oregon coast.

discrepancy exceeded the propagated NCP uncertainties during the second and third days of the deployment, and was apparent in all approaches used to calculate NCP (Sect. 2.6.3, Table 2).

While mixed layer $\Delta O_2/Ar$ primarily reflected O_2 accumulation from GPP and O_2 loss from CR, diurnal variability in [POC] was likely affected by several additional loss factors, which are discussed below. The variable difference between O_2-based and POC-based NCP measured over 3-hour increments (Eq. 11; Fig. S5) suggests that apparent POC loss rates were variable throughout the drifter period, and lower at night relative to day. Thus, the higher $NCP_{O2/Ar}$ may be attributed more to differences in daytime accumulation of POC and O_2 rather than differential POC and O_2 losses at night. Indeed, we found that differences between $CR_{O2/Ar}$ and CR_{POC} were smaller than differences in NCP or GPP throughout drifter period 1, and $CR_{O2/Ar}$ exceeded CR_{POC} during two of three nights (Fig. 5b).

In the dynamic, high productivity upwelling environment of drifter site 1, a number of processes can account for variable POC loss rates on various time scales (Gardner et al., 1999; White et al., 2017; Briggs et al., 2018). During a diatom bloom, enhanced aggregation of large silica-rich particles and zooplankton fecal pellet production can stimulate POC export and diatom cells out of the mixed layer (Buesseler, 1998; Guidi et al., 2009; Brzezinski et al., 2015; Stukel et al., 2017), progressively decreasing NCP_{POC} relative to $NCP_{O2/Ar}$. The discrepancy we observed between NCP_{POC} and $NCP_{O2/Ar}$ (up to 193 mmol C m^{-2} d^{-1}) is in the upper range of prior export estimates from various oceanic regions, including the Southern Ocean (~83 mmol C m^{-2} d^{-1}), North Atlantic spring bloom (96 mmol C m^{-2} d^{-1}) and Southern California Current system (~36 mmol C m^{-2} d^{-1}) (Henson et al., 2012; Alkire et al., 2012; Stukel et al., 2017), suggesting that POC export fluxes could comprise a significant fraction of the inferred POC loss at drifter site 1. At the same time, sub-daily changes in particle sinking velocities and size distributions could cause daytime export to exceed nighttime export (DuRand and Olson, 1998; Waite and Nodder, 2001; Oubelkheir and Sciandra, 2008; Khierrediene and Antoine, 2014; Ribalet et al., 2015; Briggs et al., 2018), leading to greater differences between $GPP_{O2/Ar}$ and GPP_{POC} than between $CR_{O2/Ar}$ and CR_{POC}, as we observed.

Another likely POC loss is DOC production through cellular exudation, viral lysis and/or grazing (Karl et al., 1998; Lochte et al., 1993; Claustre et al., 2008; Dall'Olmo et al., 2011; Briggs et al., 2018). On daily time scales, this loss term would lower NCP_{POC} relative to $NCP_{O2/Ar}$, provided that DOC production exceeds DOC respiration. Further, higher daytime net

Deleted: The global compilation of Henson et al. (2012) reported maximum export fluxes of ~83 mmol C m^{-2} d^{-1} from Southern Ocean measurements, while Alkire et al. (2012) derived maximum export fluxes of 96 mmol C m^{-2} d^{-1} during termination of the North Atlantic spring bloom. Stukel et al. (2017) applied the steady-state ^{234}Th-^{238}U approach to quantify export fluxes of ~36 mmol C m^{-2} d^{-1} in the nearshore region of the Southern California Current system. The higher value estimates are in the range of t

DOC production would cause $GPP_{O2/Ar}$ to increase more than GPP_{POC} in the daytime, while a decrease at night would cause $CR_{O2/Ar}$ to exceed CR_{POC} (Karl et al., 1998). Light- and productivity-dependent increases in DOC production in the daytime, could result, for example, from the effects of photo-respiration and other mechanisms of dissipating excess light energy (Schuback and Tortell, 2019). While we did not conduct direct measurements of DOC concentrations during the cruise, previous work in a variety of ocean environments has shown that DOC production can account for 3-37% of NCP in the Ross Sea, up to 10-40% in the equatorial Pacific Ocean, up to 66% in the Sargasso Sea during the seasonal phytoplankton bloom, and 22-40% during the North Atlantic bloom (Hansell and Carlson, 1998; Alkire et al., 2012). In the eastern Subarctic Pacific, Bif and Hansell (2019) estimated springtime ΔDOC/NCP ratios of 0.05 – 0.54 and summertime ratios of 0 – 0.28 along the Line P transect (130 – 152 °W).

In addition, assuming that DOC exudation from phytoplankton cells is positively related to growth in heterotrophic biomass (Fuhrman et al., 1985; Kuipers et al., 2000; Church et al., 2004), variations in total bacterial biomass may have impacted c_p measurements at drifter site 1 (Oubelkheir and Sciandra, 2008; Gernez et al., 2011; Barnes and Antoine, 2014). If detected by the ac-s sensor, bacteria could potentially account for some of the discrepancy between diel POC and O_2-derived variability. In particular, c_p decreases from phytoplankton exudation would counter c_p increases from heterotrophic growth. At night, this would decrease CR rates derived from c_p-based [POC], relative to O_2-derived CR rates.

A final consideration involves diurnal variation of zooplankton abundances and grazing rates, which could enhance POC loss without depleting $\Delta O_2/Ar$ (Dall'Olmo et al., 2011; White et al., 2017; Briggs et al., 2018), assuming that biomass accumulation rates from grazing surpass grazer respiration rates (Dagg et al., 1982). Further, once POC is assimilated into the body of a grazer, it joins a larger particle size class that likely exceeds the size-dependent detection limits of the beam attenuation coefficient (Stramski and Kiefer, 1991; Marra, 2002; Claustre et al., 2008;), decreasing the c_p signal used to derive POC. During our expedition, we observed a strong signature of diel migrating zooplankton based on increased nighttime signal spikes in surface optical backscatter measurements (Burt and Tortell, 2018). These effects would enhance CR_{POC} relative to $CR_{O2/Ar}$, contrary to what we observed. We thus assume that grazing at drifter site 1 is minimal relative to the effects of particle export and DOC production on GPP, CR and NCP.

Deleted: Assuming a lower bound of ~20% of NCP released as DOC yields a daily-integrated DOC flux of 21 to 33 mmol C m^{-2} d^{-1}. The remaining discrepancy between $\Delta O_2/Ar$ and POC-based NCP estimates (14 to 159 mmol C m^{-2} d^{-1}; average, 103 mmol C m^{-2} d^{-1}) is potentially attributable to particle export. Taking an upper bound of 40% of NCP as DOC production, which is closer to the easternmost station sampled in Bif and Hansell (2019), yields a daily-integrated DOC flux of 56 to 67 mmol C m^{-2} d^{-1} (Fig. 4) and a residual export flux of -14 to 126 mmol C m^{-2} d^{-1} (average, 76 mmol C m^{-2} d^{-1}) (Table 1). This range of results demonstrate that DOC production cannot likely account for the full discrepancy between $\Delta O_2/Ar$ and POC-based NCP estimates at drifter site 1, suggesting that export fluxes are likely a significant mechanism for mixed layer POC loss.¶

4.1.2 Drifter 2. Relative to the drifter 1 site, drifter site 2 exhibited similar discrepancies between $GPP_{O2/Ar}$ and GPP_{POC}, and greater discrepancies between $CR_{O2/Ar}$ and CR_{POC} (Fig. 5a-b; Table 1). Irrespective of the time of day, the rate of $\Delta O_2/Ar$ change computed over 3-hour intervals (Eq. 11) consistently exceeded POC-derived changes throughout the drifter period (Fig. S5). The strong, positive relationship between these two 3-hour measures ($p<0.05$, $r^2=0.64$), compared to the weaker correlation at drifter site 1 ($p<0.05$, $r^2= 0.39$) (Figs. 5c-d), suggests that despite large differences in the magnitude of $\Delta O_2/Ar$-derived and POC-derived GPP and CR rates, POC-based changes were a good relative indicator of O_2-derived productivity rates at drifter site 2.

Because daytime increases in both $\Delta O_2/Ar$ and [POC] were balanced by nighttime decreases, absolute differences in $NCP_{O2/Ar}$ and NCP_{POC} were smaller than at drifter site 1. This result suggests a closer coupling between primary production and heterotrophic consumption, as expected for this more oligotrophic ecosystem (Claustre et al., 2008; White et al., 2017). While the NCP discrepancy was negligible over the first 24-hour period, it increased to 32 mmol C $m^{-2}d^{-1}$ over the 24-hour period (Table 1; Fig. 4), exceeding the uncertainty of both NCP calculations. This suggests low, but non-negligible, rates of particle export, grazing and/or net DOC production at drifter site 2. Although we lack direct DOC measurements, this result is consistent with several previous observations of low net DOC production in oligotrophic waters (Bif et al., 2018; Hansell and Carlson, 1998), with values approaching ~30% of NCP in low productivity offshore waters of the Subarctic Pacific (Bif and Hansell, 2019). Low particle sinking rates could also explain the smaller absolute discrepancy between $NCP_{O2/Ar}$ and NCP_{POC} at drifter site 2. Low particle export is generally expected from phytoplankton assemblages dominated by small particle sizes <20µm, as evident in higher b_{bp} slope values and Chl-a size fractionation measurements at drifter site 2 (Sect. 3.2; Fig. 2) (Fowler and Knauer, 1986; Guidi et al., 2008).

Prior studies have observed that the amplitude of diurnal variability in $\Delta O_2/Ar$ exceeds the amplitude of diurnal variability in c_p-based [POC], as we observed at drifter site 2 (Kinkade et al., 1999; Hamme et al., 2012; Briggs et al., 2018). For example, Briggs et al. (2018) observed higher amplitude variations in O_2 relative to c_p-derived [POC] during the North Atlantic bloom, leading to higher absolute O_2-derived respiration and gross oxygen production (GOP) rates

Deleted: Therefore, the smaller differences between $NCP_{O2/Ar}$ and NCP_{POC} suggest lower, but non-negligible, absolute rates of particle export, grazing and net DOC production over consumption to decouple POC and $\Delta O_2/Ar$ dynamics at drifter site 2.

Deleted: lower 440 nm absorption values in the filtration blanks (Sect. 2.2) at drifter site 2 compared to drifter site 1 suggest lower colored dissolved organic matter concentrations (Organelli et al., 2014; Peacock et al., 2014). This

Deleted: A recent compilation of summertime DOC production and NCP measurements along the Line P transect in the Northeast Pacific Ocean, shows that DOC production comprises at most 28% of total NCP in offshore waters

Deleted: Nonetheless, POC export does occur under low productivity conditions (Durkin et al., 2015), and even small export fluxes could account for the entire discrepancy between measures of NCP at drifter site 2. For example, Durkin et al., (2015) reported significant rates of particle sinking from the small-celled, oligotrophic communities that dominate the BATS station. Finally, it is possible that grazing by zooplankton would also enhance loss of these phytoplankton cells from the mixed layer (Guidi et al., 2009). As we observed at drifter site 1, increased variability in the b_{bp} signal suggest the presence of vertically migrating zooplankton into the mixed layer during nighttime intervals of drifter period 2 (Burt and Tortell, 2018). Assuming that a maximal fraction of 28% of $NCP_{O2/Ar}$ is DOC production at drifter site 2 (Bif and Hansell, 2019), a residual POC export flux of 23 mmol C m^{-2} d^{-1} would be necessary to balance $NCP_{O2/Ar}$ and NCP_{POC} during day two of the drifter period (Table 1). This value is reasonable considering previous estimates reported from a number of lower productivity systems (Henson et al., 2012; Charette et al., 1999).

compared to c_p-derived rates. In the Southern Ocean, Hamme et al. (2012) also observed high ratios of underway ΔO_2/Ar-derived gross oxygen production to gross carbon production (i.e., GPP) based on photosynthesis-irradiance incubations. As discussed above for drifter site 1, these offsets between ΔO_2/Ar and POC-based measures might result from the effects of bacteria on c_p measurements, especially at a relatively low productivity site like drifter site 2 (Table 1; Fig. 2) (Claustre et al. 2008; Oubelkheir and Sciandra, 2008; Barnes and Antoine, 2014). Bacterial c_p variability would act to counter phytoplankton c_p variability, decreasing the magnitude of CR_{POC} relative to the magnitude of $CR_{O2/Ar}$. Indeed, the positive $CR_{O2/Ar}$ - CR_{POC} discrepancy at drifter site 2 contributed to 58-82% of the differences between ΔO_2/Ar and POC-derived GPP rates. The remaining difference may be attributed to greater daytime POC losses to the DOC pool and through particle export.

4.2 Other factors driving variability in NCP

In interpreting our results, it is important to consider a number of methodological caveats that could contribute to the apparent difference between $NCP_{O2/Ar}$ and NCP_{POC}. One important variable in all of our comparisons of productivity rates is the O_2-to-POC conversion factor, represented by the photosynthetic (PQ) and respiratory quotient (RQ). Given the relatively narrow range of possible PQ values applicable to our study sites (~1.1-1.4) (Laws 1991), variability in this term cannot account for the total discrepancy observed between ΔO_2/Ar and POC-derived GPP, CR and NCP rates. By contrast, RQ values in the ocean are more variable than PQ (Robinson and Williams, 1999; Robinson et al., 1999; Hedges et al., 2002). Therefore, variability in RQ values at both drifter sites could introduce considerable uncertainty into $GPP_{O2/Ar}$, $CR_{O2/Ar}$ and $NCP_{O2/Ar}$ calculations unaccounted for in our error propagations (Sect. 2.7). However, we found that use of RQ values ranging between 1.0 – 1.4 (Anderson and Sarmiento, 1994; Robinson and Williams, 1999; Hedges et al., 2002; Daneri et al., 2012) did not greatly change calculated $GPP_{O2/Ar}$, $CR_{O2/Ar}$, and $NCP_{O2/Ar}$ relative to GPP_{POC}, CR_{POC}, and NCP_{POC}. Therefore, it is unlikely that our selected RQ values, 1.4 and 1.1 for drifter sites 1 and 2, respectively, biased our main interpretations.

In our analysis, we interpret variations in particulate backscatter (b_{bp}) and beam attenuation (c_p) in terms of phytoplankton and total particulate organic carbon concentrations,

assuming a negligible influence of inorganic suspended minerals from various sources, including sediment resuspension and transport by the Columbia River plume (Thomas and Weatherbee, 2006). This assumption is supported by the salinity of waters we sampled at both drifter sites, which was significantly higher than that expected for river-influenced regions, (below 30 g/kg; Hickey et al., 1998). At the same time, the observed bulk refractive index of particles (η_p) at drifter site 1 do not preclude the presence of mixing between POC and a small fraction of shelf-derived inorganic particles. Estimates of η_p were generally below 1.12 for this near-shore site (Sect. 2.2; Fig. S3e), as compared to values as high as 1.26 for inorganic minerals in seawater (Lide, 1997; Twardowski et al., 2001). By comparison, calculated η_p values during the drifter 2 deployment were below 1.08, which is much closer to values expected for water-containing predominantly non-diatom phytoplankton organic carbon.

Additional uncertainty in our analysis derives from the algorithms used to estimate POC and phytoplankton carbon C_{ph} from optical measurements (Sect. 2.2). Because of particle size limitations in the optical measurements, they may not fully capture all significant size classes of the particulate pool, such as larger microplankton and zooplankton. Such a size bias in the c_p signal at 660 nm, used to derive [POC], would cause an underestimate of larger POC particles measured by beam attenuation (Claustre et al., 2008; Marra, 2002; Stramski and Kiefer, 1991), and thereby contribute to the apparent discrepancy between diel changes in [POC] and diel changes in $\Delta O_2/Ar$. Despite these potential caveats, recent work (Graff et al., 2016; Briggs et al., 2018; Burt et al., 2018) has demonstrated that c_p and b_{bp}-based derivations of [POC] and [C_{ph}] can indeed be robust in high biomass ocean regions, where productivity and the proportion of large-celled phytoplankton is significant.

Equally important, changes in the c_p-to-[POC] relationship through time could also drive apparent variability in optical [POC] estimates. The linear regression of [POC] against c_p at 660 nm measured across diverse marine environments is defined over a range of POC concentrations from ~5 to ~175 µg/L (Graff et al. 2015). At drifter site 2, POC concentrations fell within the range of this fit, and particle properties that may influence POC/c_p values (i.e., b_{bp} slope values, phytoplankton community composition, particle size and bulk refractive index) were relatively constant through time (Figs. S3d, e). By comparison, POC concentrations at drifter station 1 were 25% higher than the empirical limits of the c_p-based algorithm in Graff et al. (2015), requiring extrapolation of the POC/c_p relationship beyond its calibration range. In a limited

Deleted: However, the Columbia River plume has been observed to extend south along the coast as far as ~44.5° N in the summertime

Moved (insertion) [1]

Deleted: While these relatively high salinities support our assertion of a negligible influence of riverine particles on our measurements

Deleted: can be used to estimate the influence of inorganic minerals in our optical measurements. During drifter deployment 1, we observed median η_p values at 470, 532 and 650 nm that which

Deleted: In addition, mixing with the fresh Columbia River plume would have significantly reduced salinity at drifter site 1 to values below 30 g/kg Hickey et al., 1998). , well below the 32 g/kg we observed during this drifter deployment (Sect. 3.1; Fig. S3c), which are consistent with salinities observed in the offshore Northeast Pacific Ocean (Whitney and Freeland, 1999).

Moved up [1]: While these relatively high salinities support our assertion of a negligible influence of riverine particles on our measurements, the observed η_p values at drifter site 1 do not preclude the presence of mixing between POC and a small fraction of shelf-derived inorganic particles.

Deleted: In particular, Indeed, larger zooplankton often appear as erratic signal spikes in backscatter data (Burt and Tortell, 2018), which are typically filtered out during data processing. Moreover, the c_p signal at 660 nm, used to derive [POC], responds most strongly to particles within the 0.5–20 µm diameter range (Claustre et al., 2008; Marra, 2002; Stramski and Kiefer, 1991), which is smaller than many large diatoms, fecal pellets and particle aggregates. This

Deleted: the assumption of a constant POC/c_{p660} ratio close to the value suggested by Graff et al. (2015), is unlikely to impact the derivation [POC]-based productivity at drifter site 2, where

Deleted: (i.e., different slope of the linear fit) could apply

comparison with discrete POC samples, we found a POC–c_p slope that was similar to that of Graff et al. (albeit with a different y intercept) (Fig. S1). Nonetheless, we cannot rule out changes in the c_{p660}–[POC] relationship due to shifts in cell size and, to a lesser extent, bulk refractive index resulting from diatom accumulation (Kheireddine and Antoine, 2014; Stramski and Reynolds, 1993) (Fig. S3d–e). Indeed, Briggs et al. (2018) observed that the ratio of [POC] to c_p decreased by ~20% during the rise of the North Atlantic bloom, while values increased by ~60% during the bloom decline. If we assume a 20% decrease in POC/c_{p660} values (from ~420 to ~340 mg m^{-2}) associated with diatom growth (Briggs et al., 2018), our daily NCP_{POC} estimates would be less positive during day 1 and less negative during days 2–3. This, in turn, would increase the apparent decoupling between NCP_{POC} and $NCP_{O2/Ar}$ on days one (~27%) and three (~1%), and bring the values slightly closer on day two (~8%). Overall, the value of these potential changes is small relative to the differences we observed between $NCP_{O2/Ar}$ and NCP_{POC}, and we thus conclude that variable POC/c_{p660} ratios cannot explain the observed decoupling between POC, C_{ph} and dissolved O_2 dynamics at the drifter 1 site.

There are a number of other potential caveats in our analysis of phytoplankton carbon from b_{bp} and particle size distribution from b_{bp} slope. Previous studies have reported that daily variations in b_{bp} do not always track daily variations in c_p, suggesting that b_{bp} dynamics do not reflect phytoplankton carbon dynamics on diel time scales (Kheireddine and Antoine, 2014; Briggs et al., 2018). We observed a similar decoupling between b_{bp} and c_p in this study; for example, while c_p values at 660 nm steadily declined in the last 24 hours of drifter period 1, b_{bp} at 470 nm stayed relatively constant. Nonetheless, [C_{ph}] estimates from b_{bp} (Fig. 2) remain useful for comparisons between drifter sites, and differences in apparent phytoplankton biomass concentration were consistent with a number of the other biogeochemical differences measured between the two trophic regimes. Similarly, the relationship between b_{bp} slope and particle size distribution has been challenged in previous literature (e.g., Zeng et al., 2018). While this limits our interpretation of daily b_{bp} slope dynamics, we did find independent evidence for larger particle sizes at drifter site 1 (as predicted by the b_{bp} slope), from size fractionated [Chl-a] measurements and pigment analysis showing a greater fraction of microplankton (Sect. 3.2).

4.3 Reconciling NCP and NPP

Deleted: Finally, error associated with the POC mixing correction could affect calculated NCP_{POC} values (Eq. 8) and therefore the discrepancy between $NCP_{O2/Ar}$ and NCP_{POC}, and derived export estimates. This vertical mixing correction for NCP_{POC} is based on average parameters derived from N_2O measurements for the whole drifter period (Sect. 2.5). This introduces some error in day-to-day corrections to the NCP_{POC} calculations. In addition, the gradient term dPOC/dz in Eq. 10 is based on the difference between average POC concentrations measured at two depths during CTD deployments (5 m and one depth over 40-60 m). Because high-resolution transmissivity profiles showed that particle concentrations reached a steady minimum between 30 m and 40 m in most CTD deployments, dz in Eq. 10 was taken as the difference between the drifter 1 z_{mld} and this daily average depth of minimum transmissivity, rather than the deeper POC sampling depth (i.e., 40 – 60 m). Because variations in transmissivity do not necessarily equate to variations in [POC], errors in dz would impact the vertical mixing correction and therefore calculated NCP_{POC} values. For example, if the [POC] minimum was actually deeper, this would increase the value of dz and decrease dPOC/dz and the total mixing correction, yielding lower NCP_{POC} values and a higher discrepancy between NCP measures. In propagating the error for NCP_{POC}, we have included the standard deviation of the minimum transmissivity depth across daily CTD casts, which partially addresses this uncertainty in the dz term. Fortunately, the NCP_{POC} mixing corrections over drifter period 1 approximate the magnitude of the $NCP_{O2/Ar}$ mixing correction (Sect. 3.3, Table 1), increasing our confidence in the POC mixing correction applied here.¶
Aside from uncertainties that directly impact estimates of NCP, t

During both drifter surveys, we estimated daily-integrated net primary productivity (NPP) values using carbon-based production model (CbPM) calculations and ^{14}C bottle incubations (Sect. 2.5). On several days, these two estimates of NPP were consistently lower than $NCP_{O2/Ar}$ integrated over the same time scales and mixed layer depths (Table 1). Similarly, Briggs et al. (2018) and Alkire et al. (2012) also reported NCP values that were equal to or greater than NPP values obtained from different methodologies during their Lagrangian study of the North Atlantic Bloom.

In theory, NCP cannot exceed NPP, as NCP includes additional respiration terms not included in NPP, and must always be equal to or (more realistically) lower than NPP. Recent work in the Northeast Pacific Ocean, has reported mean NCP/NPP ratios, based on $\Delta O_2/Ar$ measurements and CbPM calculations, ranging from 0.16 to 0.26 in offshore and coastal waters (Burt et al., 2018). These values, determined from continuous observations along a moving ship-track, are consistent with theoretical expectations. The observed high (>1) apparent NCP/NPP values observed in our study and that of Briggs et al. (2018) and Alkire et al. (2012) highlight a number of methodological limitations that could depress NPP estimates.

One possibility, which has been discussed at length by various authors (Gieskes et al., 1979; Fogg and Calvario-Martinez, 1989; Marra, 2009), is that bottle containment effects limit accurate estimates of ^{14}C uptake. This effect would have caused underestimates of ^{14}C-NPP during both drifter surveys, relative to CbPM-NPP and $NCP_{O2/Ar}$, which do not require discrete sample incubations. In addition, during the last ^{14}C-uptake experiment of drifter survey 2, the incubator warmed (as the ship passed through warm SST water used to cool the tanks), potentially creating heat stress on phytoplankton and depressing ^{14}C-NPP values.

A number of factors may also influence CbPM-based NPP estimates. While the model applies a satellite-based relationship between [Chl-a]/[C_{ph}] and daily mixed layer irradiance (E_g) to calculate growth rate, these E_g values may not fully parametrize phytoplankton physiology for mixed assemblages in the ocean (Westberry et al., 2008). Indeed, phytoplankton photophysiology varies with other environmental conditions and phytoplankton composition (Cloern et al., 1995; Geider et al., 1998; MacIntyre et al., 2002; Westberry et al., 2008). In addition, the CbPM does not allow calculated growth rates to exceed 2 d^{-1}, which may not apply to all ocean environments (Graff et al., 2016). These uncertainties could potentially impact the applicability of the CbPM parameters to the specific ocean conditions at drifter sites 1 and 2. In

addition, a vertical mixing correction for ac-s and backscatter-derived [Chl-a] and [C_{ph}], respectively, not feasible in the present data set, may improve CbPM-based estimates of NPP.

5 Conclusions

In the current study, biological oxygen saturation ($\Delta O_2/Ar$) and optically-derived particulate organic carbon (POC) were measured continuously and simultaneously during two Lagrangian drifter deployments. This dual measurement approach facilitated direct comparison of O_2/Ar and POC-derived measures of gross primary productivity (GPP), community respiration (CR), and net community production (NCP), from a mesotrophic upwelling-influenced system and a more oligotrophic system further offshore. As hypothesized, the results show that O_2 and POC-based measures of GPP and NCP diverge in mid-to-high productivity phytoplankton communities, where daily fluctuations in $\Delta O_2/Ar$ are decoupled from POC cycling. Interestingly, oxygen-based GPP and CR also exceeded POC-based GPP and CR rates at the lower productivity site, though we found that net changes in POC scaled with $\Delta O_2/Ar$-based productivity estimates, suggesting a tighter coupling between O_2 and POC cycles.

These findings are generally consistent with current understanding of productivity dynamics and mixed layer POC cycling in these two coastal Pacific environments, and complement only one prior comparison of daily GPP and NCP estimates from simultaneous, autonomous measurements of c_p and O_2 in the North Atlantic mixed layer (Alkire et al., 2012; Briggs et al., 2018). Importantly, however, our results differ from earlier studies by providing two examples of significant disagreement between $GPP_{O2/Ar}$ and GPP_{POC}, and $CR_{O2/Ar}$ and CR_{POC}, likely resulting from sub-daily variations in particle export, net DOC production, and bacterial growth over respiration. In such cases, assuming constant daily respiration rates by extrapolating nighttime rates of change may pose challenges for comparing $\Delta O_2/Ar$ and POC-based GPP and CR. We have further shown that for upwelling regions like drifter site 1, it is important to account for vertical mixing of sub-surface waters into the mixed layer, and its effect on not only $NCP_{O2/Ar}$ calculations (Izett et al., 2018), but also on NCP_{POC} estimates through dilution of the surface POC signature. Our study thus illustrates an application of the vertical mixing coefficient, k_{mix}, derived from [N_2O] profiles to more accurately estimate net changes in POC and nutrient concentration in such environments.

Deleted: ¶
4.4 Comparison to other studies¶
¶
A number of previous studies have examined diurnal variation in upper ocean phytoplankton and organic particle dynamics across a variety of productivity regimes, from oligotrophic environments (Claustre et al., 1999, 2008; Wu et al., 2010; Gernez et al., 2011; Kheireddine and Antoine, 2014; Thyssen et al., 2014; Nicholson et al., 2015; Ribalet et al., 2015; White et al., 2017), to higher productivity waters and phytoplankton blooms (Brunet and Lizon, 2003; Wu et al., 2010; Alkire et al., 2012; Gernez et al., 2011; Dugenne et al., 2014; Kheireddine and Antoine, 2014; Needham and Fuhrman, 2016; Briggs et al., 2018). In general, these studies have shown that more productive environments exhibit higher amplitude diurnal variations in beam attenuation, POC concentration, phytoplankton cell abundances, Chl-a, and metabolic rates, as compared to oligotrophic regions. These prior results are consistent with the differences we observed between the two distinct Northeast Pacific trophic environments represented by drifter sites 1 and 2, respectively (Sect. 3.2; Figs. 2, S5). ¶
To our knowledge, however, only two previous studies have directly compared diurnal variations in O_2-based and c_p-based mixed layer productivity using Lagrangian drifters (Alkire et al., 2012; Briggs et al., 2018). This previous work demonstrated that GPP and NCP dynamics derived from dissolved O_2 measurements differed from net POC accumulation over the course of the North Atlantic bloom, with the magnitude of this disparity varying as a function of bloom stage. The authors found that highest rates of POC export and DOC production, corresponding to the greatest O_2-POC discrepancy, occurred during the main period of the bloom development, prior to its termination. The results of our study off the Oregon coast extend these previous observations from the North Atlantic bloom into two new surface ocean regimes: a high productivity Pacific upwelling zone, and a lower productivity offshore region. The upwelling environment was characterized by rapid diatom accumulation, yielding significant differences between $NCP_{O2/Ar}$ and NCP_{POC}, and $GPP_{O2/Ar}$ and GPP_{POC}. We also observed significant differences between $\Delta O_2/Ar$-based and POC-based GPP and CR rates at the lower productivity drifter 2 site, even though daily-integrated measures of NCP and net carbon accumulation agreed more closely. ¶
¶
While most previous work across oligotrophic environments has highlighted the agreement between GPP derived from daily variability in beam attenuation and dissolved O_2 (e.g., Claustre et al., 2008; White et al., 2017), our results illustrate two different examples where $\Delta O_2/Ar$-based and POC-based GPP rates do not agree. In future work, measurements that simultaneously estimate surface water O_2 accumulation, net DOC production and vertical transport of deep water to the mixed layer at high temporal resolution offer the opportunity to evaluate the fate of NCP. ¶
that even lower productivity environments like drifter site 2 can display a quantifiable discrepancy between productivity measures. At the same time, while POC-derived GPP and CR consistently underestimated $\Delta O_2/Ar$-derived rates, net changes in [POC] were a sufficient relative indicator of variations in $\Delta O_2/Ar$-based productivity, as has been ... [1]

Moving forward, the disparity between POC and O_2-based NCP estimates offers an opportunity to continuously track cumulative POC losses in the mixed layer using autonomous ship-board or in situ sensors. As it is labor intensive to measure POC export on short time scales with sediment traps and the ^{234}Th-^{238}U disequilibrium method (Buesseler et al., 2006; Savoye et al., 2006), simultaneous underway measurements of dissolved O_2, particulate beam attenuation and CDOM absorption and spectral slope over a range of wavelengths <400 nm (Del Vecchio and Blough, 2004; Grunert et al., 2018) may provide a valuable, first-order approximation of POC partitioning among living phytoplankton biomass, particle export and dissolved organic carbon (DOC) in the surface ocean on short time scales. At drifter site 1, for example, taking an upper bound of 40% of NCP as DOC production (close to the fraction estimated Alkire et al. (2012) during the North Atlantic spring bloom) yields a 3-day average DOC flux of 55 mmol C m^{-2} d^{-1} and residual export flux of 76 mmol C m^{-2} d^{-1}. Being able to estimate such quantities with this approach is especially important in the California coastal upwelling regime and other similar ecosystems with high NCP and significant potential for carbon transfer to higher trophic levels.

For future work, we recommend a number of approaches to facilitate estimation of POC export from coupled O_2, POC, and DOC dynamics. First, it will be valuable to constrain particle size, and partitioning of POC into detrital and living (phytoplankton and heterotrophic bacteria) components to properly assess the size range captured by optically-derived POC and C_{ph} measurements. Second, independent estimates of POC export and DOC concentrations during each drifter deployment could validate POC export fluxes derived from coupled O_2 and POC measurements. Relatedly, depth-resolved backscatter profiles (Briggs et al., 2013, 2018) could be used as another autonomous approach to calculating export fluxes, as an independent check on surface-based estimates. Going forward, there is significant future potential to exploit coupled O_2 and c_p measurements on autonomous platforms, including various ocean moorings (e.g., the Optical Dynamics Experiment, the Biowatt II program, and the Bermuda Testbed Mooring program), and biogeochemical floats and gliders to resolve opportunistic, high-resolution POC export time series (Stramska and Dickey, 1992; Kinkade et al., 1999; Dickey and Chang, 2002). Deployment of such autonomous measurement systems across a range of oceanic regions will help to constrain POC and productivity dynamics on global scales.

Deleted: The results show that this approach performs well in distinguishing regions of high particle export, notwithstanding some major methodological limitations (Sect. 4.2) and poorly constrained DOC production rates (Sect. 4.1.1), which increase the uncertainty of our export estimates at drifter site 1.

Data availability

Discrete and underway optical measurements may be accessed at https://github.com/srosengard/rosengard-tortell-oc2017.git

Author contributions

Sarah Rosengard, Philippe Tortell, and Nina Schuback collected the data in the field. Robert Izett processed the CTD cast data and measured nitrous oxide concentrations in discrete samples. Sarah Rosengard wrote the manuscript with significant input from the co-authors.

Competing interests

The authors declare that they have no conflict of interest.

Acknowledgements

Special thanks to Jessie Gwinn, Ross McCulloch, Chen Zeng, Melissa Beaulac, Chris Payne and Maureen Soon for assistance in field collection and analysis of samples, and to two anonymous reviewers for insightful suggestions on earlier versions of this manuscript. This project was funded by the Natural Sciences and Engineering Research Council of Canada (NSERC), and by the US National Science Foundation (NSF project number 1436344).

References

Alkire, M. B., D'Asaro, E., Lee, C., Jane Perry, M., Gray, A., Cetinić, I., Briggs, N., Rehm, E., Kallin, E., Kaiser, J. and González-Posada, A.: Estimates of net community production and export using high-resolution, Lagrangian measurements of O2, NO3−, and POC through the evolution of a spring diatom bloom in the North Atlantic, Deep Sea Res. Part I Oceanogr. Res. Pap., 64, 157–174, doi:10.1016/j.dsr.2012.01.012, 2012.

Anderson, L. A., and Sarmiento, J. L.: Redfield ratios of remineralization determined by nutrient data analysis, Global biogeochem. cycles, 8(1), 65-80, 1994.

Barnes, M., and Antoine, D.: Proxies of community production derived from the diel variability of particulate attenuation and backscattering coefficients in the northwest Mediterranean Sea, Limnol. Oceanogr., 59(6), 2133-2149, 2014.

Behrenfeld, M. J., Boss, E., Siegel, D. A. and Shea, D. M.: Carbon-based ocean productivity and phytoplankton physiology from space, Global Biogeochem. Cycles, 19(1), 2005.

Bif, M. B. and Hansell, D. A.: Seasonality of dissolved organic carbon in the upper Northeast Pacific Ocean, Global Biogeochem. Cycles, 2019.

Bif, M. B., Hansell, D. A. and Popendorf, K. J.: Controls on the fate of dissolved organic carbon under contrasting upwelling conditions, Front. Mar. Sci., 5, 463, 2018.

Boss, E., Twardowski, M. S. and Herring, S.: Shape of the particulate beam attenuation spectrum and its inversion to obtain the shape of the particulate size distribution, Appl. Opt., 40(27), 4885–4893, 2001.

de Boyer Montégut, C., Madec, G., Fischer, A. S., Lazar, A. and Iudicone, D.: Mixed layer depth over the global ocean: An examination of profile data and a profile-based climatology, J. Geophys. Res., 109(C12), C12003, doi:10.1029/2004JC002378, 2004.

Briggs, N., Guðmundsson, K., Cetinić, I., D'Asaro, E., Rehm, E., Lee, C. and Perry, M. J.: A multi-method autonomous assessment of primary productivity and export efficiency in the springtime North Atlantic, Biogeosciences, 15(14), 4515–4532, 2018.

Briggs, N. T., Slade, W. H., Boss, E. and Perry, M. J.: Method for estimating mean particle size from high-frequency fluctuations in beam attenuation or scattering measurements, Appl. Opt., 52(27), 6710–6725, 2013.

Brunet, C. and Lizon, F.: Tidal and diel periodicities of size-fractionated phytoplankton pigment signatures at an offshore station in the southeastern English Channel, Estuar. Coast. Shelf Sci., 56(3–4), 833–843, 2003.

Brzezinski, M., Villareal, T. and Lipschultz, F.: Silica production and the contribution of diatoms to new and primary production in the central North Pacific, Mar. Ecol. Prog. Ser., 167, 89–104, doi:10.3354/meps167089, 1998.

Brzezinski, M. A.: The Si:C:N ratio of marine diatoms: Interspecific variability and the effect of some environmental variables, J. Phycol., 21(3), 347–357, doi:10.1111/j.0022-3646.1985.00347.x, 2004.

Brzezinski, M. A., Krause, J. W., Bundy, R. M., Barbeau, K. A., Franks, P., Goericke, R.,

Landry, M. R. and Stukel, M. R.: Enhanced silica ballasting from iron stress sustains carbon export in a frontal zone within the California Current, J. Geophys. Res. Ocean., 120(7), 4654–4669, 2015.

Buesseler, K. O.: The decoupling of production and particulate export in the surface ocean, Global Biogeochem. Cycles, 12(2), 297–310, 1998.

Buesseler, K. O., Benitez-Nelson, C. R., Moran, S. B., Burd, A., Charette, M., Cochran, J. K., Coppola, L., Fisher, N. S., Fowler, S. W. and Gardner, W. D.: An assessment of particulate organic carbon to thorium-234 ratios in the ocean and their impact on the application of 234Th as a POC flux proxy, Mar. Chem., 100(3–4), 213–233, 2006.

Burt, W. J. and Tortell, P. D.: Observations of Zooplankton Diel Vertical Migration From High-Resolution Surface Ocean Optical Measurements, Geophys. Res. Lett., 45(24), 13–396, 2018.

Burt, W. J., Westberry, T. K., Behrenfeld, M. J., Zeng, C., Izett, R. W. and Tortell, P. D.: Carbon: Chlorophyll Ratios and Net Primary Productivity of Subarctic Pacific Surface Waters Derived From Autonomous Shipboard Sensors, Global Biogeochem. Cycles, 32(2), 267–288, doi:10.1002/2017GB005783, 2018.

Capelle, D. W., Dacey, J. W. and Tortell, P. D.: An automated, high through-put method for accurate and precise measurements of dissolved nitrous-oxide and methane concentrations in natural waters, Limnol. Oceanogr. Methods, 13(7), 345–355, 2015.

Cassar, N., Barnett, B. A., Bender, M. L., Kaiser, J., Hamme, R. C. and Tilbrook, B.: Continuous high-frequency dissolved O2/Ar measurements by equilibrator inlet mass spectrometry, Anal. Chem., 81(5), 1855–1864, 2009.

Cassar, N., Nevison, C. D. and Manizza, M.: Correcting oceanic O2/Ar-net community production estimates for vertical mixing using N2O observations, Geophys. Res. Lett., 41(24), 8961–8970, 2014.

Church, M. J., Ducklow, H. W., and Karl, D. M.: Light dependence of [3H] leucine incorporation in the oligotrophic North Pacific Ocean, Appl. Environ. Microbiol., 70(7), 4079-4087, 2004.

Claustre, H., Morel, A., Babin, M., Cailliau, C., Marie, D., Marty, J., Tailliez, D. and Vaulot, D.: Variability in particle attenuation and chlorophyll fluorescence in the tropical Pacific: Scales, patterns, and biogeochemical implications, J. Geophys. Res. Ocean., 104(C2), 3401–3422, 1999.

Claustre, H., Huot, Y., Obernosterer, I., Gentili, B., Tailliez, D. and Lewis, M.: Gross community

production and metabolic balance in the South Pacific Gyre, using a non intrusive bio-optical method, Biogeosciences, 5, 463-474, 2008.
Cloern, J. E., Grenz, C. and Vidergar-Lucas, L.: An empirical model of the phytoplankton chlorophyll: carbon ratio-the conversion factor between productivity and growth rate, Limnol. Oceanogr., 40(7), 1313–1321, 1995.
Dagg, M. J., Vidal, J., Whitledge, T. E., Iverson, R. L. and Goering, J. J.: The feeding, respiration, and excretion of zooplankton in the Bering Sea during a spring bloom, Deep Sea Res. Part A. Oceanogr. Res. Pap., 29(1), 45–63, 1982.
Dall'Olmo, G., Boss, E., Behrenfeld, M. J., Westberry, T. K., Courties, C., Prieur, L., Pujo-Pay, M., Hardman-Mountford, N. and Moutin, T.: Inferring phytoplankton carbon and eco-physiological rates from diel cycles of spectral particulate beam-attenuation coefficient, Biogeosciences, 8(11), 3423–3439, 2011.
Daneri, G., Lizárraga, L., Montero, P., González, H. E., and Tapia, F. J.: Wind forcing and short-term variability of phytoplankton and heterotrophic bacterioplankton in the coastal zone of the Concepción upwelling system (Central Chile), Prog. Oceanogr., 92, 92-96, 2012.
Del Vecchio, R., and Blough, N. V.: Spatial and seasonal distribution of chromophoric dissolved organic matter and dissolved organic carbon in the Middle Atlantic Bight, Mar. Chem., 89(1-4), 169-187, 2004.
Dickey, T. D. and Chang, G. C.: Recent advances and future visions: temporal variability of optical and bio-optical properties of the ocean, Oceanogr. DC-OCEANOGRAPHY Soc., 14(3), 15–29, 2002.
Dugenne, M., Thyssen, M., Nerini, D., Mante, C., Poggiale, J.-C., Garcia, N., Garcia, F. and Grégori, G. J.: Consequence of a sudden wind event on the dynamics of a coastal phytoplankton community: an insight into specific population growth rates using a single cell high frequency approach, Front. Microbiol., 5, 485, 2014.
Durand, M. D., and Olson, R. J.: Diel patterns in optical properties of the chlorophyte Nannochloris sp.: Relating individual-cell to bulk measurements, Limnol. Oceanogr., 43(6), 1107-1118, 1998.
Fernández-Urruzola, I., Osma, N., Packard, T. T., Gómez, M., and Postel, L.: Distribution of zooplankton biomass and potential metabolic activities across the northern Benguela upwelling system, J Marine Syst, 140, 138-149, 2014.

Ferrón, S., Wilson, S. T., Martínez-García, S., Quay, P. D., and Karl, D. M.: Metabolic balance in the mixed layer of the oligotrophic North Pacific Ocean from diel changes in O2/Ar saturation ratios, Geophys. Res. Lett., 42(9), 3421-3430, 2015.

Fogg, G. E. and Calvario-Martinez, O.: Effects of bottle size in determinations of primary productivity by phytoplankton, Hydrobiologia, 173(2), 89–94, doi:10.1007/BF00015518, 1989.

Fowler, S. W. and Knauer, G. A.: Role of large particles in the transport of elements and organic compounds through the oceanic water column, Prog. Oceanogr., 16(3), 147–194, doi:10.1016/0079-6611(86)90032-7, 1986.

Fuhrman, J. A., Eppley, R. W., Hagström, Å., and Azam, F.: Diel variations in bacterioplankton, phytoplankton, and related parameters in the Southern California Bight, Mar. Ecol. Prog. Ser, 27, 9-20, 1985.

Garcia, H. E. and Gordon, L. I.: Oxygen solubility in seawater: Better fitting equations, Limnol. Oceanogr., 37(6), 1307–1312, 1992.

Gardner, W. D., Walsh, I. D. and Richardson, M. J.: Biophysical forcing of particle production and distribution during a spring bloom in the North Atlantic, Deep Sea Res. Part II Top. Stud. Oceanogr., 40(1–2), 171–195, 1993.

Geider, R. J., Maclntyre, H. L. and Kana, T. M.: A dynamic regulatory model of phytoplanktonic acclimation to light, nutrients, and temperature, Limnol. Oceanogr., 43(4), 679–694, 1998.

Gernez, P., Antoine, D. and Huot, Y.: Diel cycles of the particulate beam attenuation coefficient under varying trophic conditions in the northwestern Mediterranean Sea: Observations and modeling, Limnol. Oceanogr., 56(1), 17–36, 2011.

Gieskes, W. W. C., Kraay, G. W. and Baars, M. A.: Current 14C methods for measuring primary production: Gross underestimates in oceanic waters, Netherlands J. Sea Res., 13(1), 58–78, doi:10.1016/0077-7579(79)90033-4, 1979.

Graff, J. R., Westberry, T. K., Milligan, A. J., Brown, M. B., Dall'Olmo, G., Dongen-Vogels, V. van, Reifel, K. M. and Behrenfeld, M. J.: Analytical phytoplankton carbon measurements spanning diverse ecosystems, Deep Sea Res. Part I Oceanogr. Res. Pap., 102, 16–25, doi:10.1016/J.DSR.2015.04.006, 2015.

Graff, J. R., Westberry, T. K., Milligan, A. J., Brown, M. B., Olmo, G. D., Reifel, K. M. and Behrenfeld, M. J.: Photoacclimation of natural phytoplankton communities, Mar. Ecol. Prog. Ser., 542, 51–62, 2016.

Grunert, B. K., Mouw, C. B., and Ciochetto, A. B.: Characterizing CDOM spectral variability across diverse regions and spectral ranges, Global Biogeochem. Cycles, 32(1), 57-77, 2018.
Guidi, L., Jackson, G. A., Stemmann, L., Carlos Miquel, J., Picheral, M. and Gorsky, G.: Author's personal copy Relationship between particle size distribution and flux in the mesopelagic zone, , doi:10.1016/j.dsr.2008.05.014, 2008.
Guidi, L., Stemmann, L., Jackson, G. A., Ibanez, F., Claustre, H., Legendre, L., Picheral, M. and Gorskya, G.: Effects of phytoplankton community on production, size, and export of large aggregates: A world-ocean analysis, Limnol. Oceanogr., 54(6), 1951–1963, 2009.
Hamme, R. C., Cassar, N., Lance, V. P., Vaillancourt, R. D., Bender, M. L., Strutton, P. G., Moore, T. S., DeGrandpre, M. D., Sabine, C. L. and Ho, D. T.: Dissolved O2/Ar and other methods reveal rapid changes in productivity during a Lagrangian experiment in the Southern Ocean, J. Geophys. Res. Ocean., 117(C4), 2012.
Hansell, D. A. and Carlson, C. A.: Net community production of dissolved organic carbon, Global Biogeochem. Cycles, 12(3), 443–453, 1998.
Hedges, J. I., Baldock, J. A., Gélinas, Y., Lee, C., Peterson, M. L., and Wakeham, S. G.: The biochemical and elemental compositions of marine plankton: A NMR perspective, Mar. Chem., 78(1), 47-63, 2002.
Henson, S. A., Sanders, R. and Madsen, E.: Global patterns in efficiency of particulate organic carbon export and transfer to the deep ocean, Global Biogeochem. Cycles, 26(1), 2012.
Hickey, B. M., Pietrafesa, L. J., Jay, D. A. and Boicourt, W. C.: The Columbia River plume study: Subtidal variability in the velocity and salinity fields, J. Geophys. Res. Ocean., 103(C5), 10339–10368, 1998.
Hirata, T., Hardman-Mountford, N. J., Brewin, R. J. W., Aiken, J., Barlow, R., Suzuki, K., Isada, T., Howell, E., Hashioka, T. and Noguchi-Aita, M.: Synoptic relationships between surface Chlorophyll-a and diagnostic pigments specific to phytoplankton functional types, Biogeosciences, 8(2), 311–327, 2011.
Hopkinson, B. M., and Barbeau, K.A.: Organic and redox speciation of iron in the eastern tropical North Pacific suboxic zone, Mar. Chem., 106(1-2), 2-17, 2007.
Hoppe, C. J. M., Schuback, N., Semeniuk, D. M., Maldonado, M. T. and Rost, B.: Functional Redundancy Facilitates Resilience of Subarctic Phytoplankton Assemblages toward Ocean Acidification and High Irradiance , Front. Mar. Sci. , 4, 229 [online] Available from:

https://www.frontiersin.org/article/10.3389/fmars.2017.00229, 2017.
Izett, R. W., Manning, C. C., Hamme, R. C. and Tortell, P. D.: Refined estimates of net community production in the Subarctic Northeast Pacific derived from ΔO2/Ar measurements with N2O-based corrections for vertical mixing, Global Biogeochem. Cycles, 32(3), 326–350, 2018.
Jin, X., Najjar, R. G., Louanchi, F. and Doney, S. C.: A modeling study of the seasonal oxygen budget of the global ocean, J. Geophys. Res. Ocean., 112(C5), 2007.
Kaiser, J., Reuer, M. K., Barnett, B. and Bender, M. L.: Marine productivity estimates from continuous O2/Ar ratio measurements by membrane inlet mass spectrometry, Geophys. Res. Lett., 32(19), 2005.
Karl, D. M., Hebel, D. V., Björkman, K., and Letelier, R. M.: The role of dissolved organic matter release in the productivity of the oligotrophic North Pacific Ocean, Limnol. Oceanogr., 43(6), 1270-1286, 1998.
Keeling, R. F. and Shertz, S. R.: Seasonal and interannual variations in atmospheric oxygen and implications for the global carbon cycle, Nature, 358(6389), 723, 1992.
Kheireddine, M. and Antoine, D.: Diel variability of the beam attenuation and backscattering coefficients in the northwestern Mediterranean Sea (BOUSSOLE site), J. Geophys. Res. Ocean., 119(8), 5465–5482, 2014.
Kinkade, C. S., Marra, J., Dickey, T. D., Langdon, C., Sigurdson, D. E. and Weller, R.: Diel bio-optical variability observed from moored sensors in the Arabian Sea, Deep sea Res. Part II Top. Stud. Oceanogr., 46(8–9), 1813–1831, 1999.
Kostadinov, T. S., Siegel, D. A. and Maritorena, S.: Retrieval of the particle size distribution from satellite ocean color observations, J. Geophys. Res., 114(C9), C09015, doi:10.1029/2009JC005303, 2009.
Kuipers, B., van Noort, G. J., Vosjan, J., and Herndl, G. J.: Diel periodicity of bacterioplankton in the euphotic zone of the subtropical Atlantic Ocean, Mar. Ecol. Prog. Ser., 201, 13-25, 2000.
Laws, E. A.: Photosynthetic quotients, new production and net community production in the open ocean, Deep Sea Res. Part A. Oceanogr. Res. Pap., 38(1), 143–167, 1991.
Lide, D. R.: Physical and optical properties of minerals, CRC Handb. Chem. Phys., 4–130, 1997.
Lochte, K., Ducklow, H. W., Fasham, M. J. R. and Stienen, C.: Plankton succession and carbon cycling at 47 N 20 W during the JGOFS North Atlantic Bloom Experiment, Deep Sea Res. Part

II Top. Stud. Oceanogr., 40(1–2), 91–114, 1993.
Loisel, H., Nicolas, J.-M., Sciandra, A., Stramski, D. and Poteau, A.: Spectral dependency of optical backscattering by marine particles from satellite remote sensing of the global ocean, J. Geophys. Res., 111(C9), C09024, doi:10.1029/2005JC003367, 2006.
Lønborg, C., Martínez-García, S., Teira, E., and Álvarez-Salgado, X. A.: Bacterial carbon demand and growth efficiency in a coastal upwelling system, Aquat. Microb. Ecol., 63(2), 183-191, 2011.
MacIntyre, H. L., Kana, T. M., Anning, T. and Geider, R. J.: Photoacclimation of irradiance response curves and photosynthetic pigments in microalgae and cyanobacteria, J. Phycol., 38(1), 17–38, doi:10.1046/j.1529-8817.2002.00094.x, 2002.
Manning, C. C., Stanley, R. H. R., Nicholson, D. P., Smith, J. M., Pennington, J. T., Fewings, M. R., Squibb, M. E. and Chavez, F. P.: Impact of recently upwelled water on productivity investigated using in situ and incubation-based methods in Monterey Bay, J. Geophys. Res. Ocean., 122(3), 1901–1926, 2017.
Marra, J.: Approaches to the measurement of plankton production, Phytoplankt. Product. Carbon Assim. Mar. Freshw. Ecosyst., 78–108, 2002.
Marra, J.: Net and gross productivity: weighing in with 14C, Aquat. Microb. Ecol., 56(2–3), 123–131, doi:10.3354/ame01306, 2009.
Morel, A., Huot, Y., Gentili, B., Werdell, P. J., Hooker, S. B. and Franz, B. A.: Examining the consistency of products derived from various ocean color sensors in open ocean (Case 1) waters in the perspective of a multi-sensor approach, Remote Sens. Environ., 111(1), 69–88, 2007.
Murphy, J. and Riley, J. P.: A modified single solution method for the determination of phosphate in natural waters, Anal. Chim. Acta, 27, 31–36, 1962.
Needham, D. M. and Fuhrman, J. A.: Pronounced daily succession of phytoplankton, archaea and bacteria following a spring bloom, Nat. Microbiol., 1(4), 16005, 2016.
Nicholson, D. P., Wilson, S. T., Doney, S. C. and Karl, D. M.: Quantifying subtropical North Pacific gyre mixed layer primary productivity from Seaglider observations of diel oxygen cycles, Geophys. Res. Lett., 42(10), 4032–4039, 2015.
Oubelkheir, K., and Sciandra, A.: Diel variations in particle stocks in the oligotrophic waters of the Ionian Sea (Mediterranean), J. Marine Syst., 74(1-2), 364-371, 2008.
Raymond, P. A., Zappa, C. J., Butman, D., Bott, T. L., Potter, J., Mulholland, P., Laursen, A. E.,

McDowell, W. H. and Newbold, D.: Scaling the gas transfer velocity and hydraulic geometry in streams and small rivers, Limnol. Oceanogr. Fluids Environ., 2(1), 41–53, 2012.
Reuer, M. K., Barnett, B. A., Bender, M. L., Falkowski, P. G. and Hendricks, M. B.: New estimates of Southern Ocean biological production rates from O2/Ar ratios and the triple isotope composition of O2, Deep Sea Res. Part I Oceanogr. Res. Pap., 54(6), 951–974, 2007.
Ribalet, F., Swalwell, J., Clayton, S., Jiménez, V., Sudek, S., Lin, Y., Johnson, Z. I., Worden, A. Z. and Armbrust, E. V.: Light-driven synchrony of Prochlorococcus growth and mortality in the subtropical Pacific gyre, Proc. Natl. Acad. Sci., 112(26), 8008–8012, 2015.
Riley, J. P.: Grasshoff, K. [Ed.] 1976. Methods of seawater analysis. Verlag Chemie, Weinheim and New York, xv+ 317 p. $43.60., 1977.
Robinson, C., and Williams, P. J. L. B.: Plankton net community production and dark respiration in the Arabian Sea during September 1994, Deep Sea Res. Part II Top. Stud. Oceanogr., 46(3-4), 745-765, 1999.
Robinson, C., Archer, S. D., and Williams, P. J. L. B.: Microbial dynamics in coastal waters of East Antarctica: plankton production and respiration, Mar. Ecol. Prog. Ser., 180, 23-36, 1999.
Robinson, C., Serret, P., Tilstone, G., Teira, E., Zubkov, M. V., Rees, A. P., and Woodward, E. M. S.: Plankton respiration in the eastern Atlantic Ocean, Deep Sea Res. Part I Oceanogr. Res. Pap., 49(5), 787-813, 2002.
Roesler, C. S. and Barnard, A. H.: Optical proxy for phytoplankton biomass in the absence of photophysiology: Rethinking the absorption line height, Methods Oceanogr., 7, 79–94, 2013.
Savoye, N., Benitez-Nelson, C., Burd, A. B., Cochran, J. K., Charette, M., Buesseler, K. O., Jackson, G. A., Roy-Barman, M., Schmidt, S. and Elskens, M.: 234Th sorption and export models in the water column: a review, Mar. Chem., 100(3–4), 234–249, 2006.
Schuback, N., and Tortell, P. D.: Diurnal regulation of photosynthetic light absorption, electron transport and carbon fixation in two contrasting oceanic environments, Biogeosciences, 16(7), 1381-1399, 2019.
Schuback, N., Flecken, M., Maldonado, M. T. and Tortell, P. D.: Diurnal variation in the coupling of photosynthetic electron transport and carbon fixation in iron-limited phytoplankton in the NE subarctic Pacific, Biogeosciences, 13, 1019–1035, doi:10.5194/bg-13-1019-2016, 2016.
Siegel, D. A., Dickey, T. D., Washburn, L., Hamilton, M. K. and Mitchell, B. G.: Optical

determination of particulate abundance and production variations in the oligotrophic ocean, Deep Sea Res. Part A. Oceanogr. Res. Pap., 36(2), 211–222, 1989.
Stanley, R. H. R., Kirkpatrick, J. B., Cassar, N., Barnett, B. A. and Bender, M. L.: Net community production and gross primary production rates in the western equatorial Pacific, Global Biogeochem. Cycles, 24(4), 2010.
Stramska, M. and Dickey, T. D.: Short-term variations of the bio-optical properties of the ocean in response to cloud-induced irradiance fluctuations, J. Geophys. Res. Ocean., 97(C4), 5713–5721, 1992.
Stramska, M. and Dickey, T. D.: Modeling phytoplankton dynamics in the northeast Atlantic during the initiation of the spring bloom, J. Geophys. Res. Ocean., 99(C5), 10241–10253, 1994.
Stramska, M., Stramski, D., Hapter, R., Kaczmarek, S. and Ston´, J. S.: Bio-optical relationships and ocean color algorithms for the north polar region of the Atlantic, J. Geophys. Res, 108(C5), 3143, doi:10.1029/2001JC001195, 2003.
Stramski, D. and Kiefer, D. A.: Light scattering by microorganisms in the open ocean, Prog. Oceanogr., 28(4), 343–383, doi:10.1016/0079-6611(91)90032-H, 1991.
Stramski, D. and Reynolds, R. A.: Diel variations in the optical properties of a marine diatom, Limnol. Oceanogr., 38(7), 1347–1364, 1993.
Stukel, M. R., Aluwihare, L. I., Barbeau, K. A., Chekalyuk, A. M., Goericke, R., Miller, A. J., Ohman, M. D., Ruacho, A., Song, H. and Stephens, B. M.: Mesoscale ocean fronts enhance carbon export due to gravitational sinking and subduction, Proc. Natl. Acad. Sci., 114(6), 1252–1257, 2017.
Sullivan, J. M., Twardowski, M. S., Donaghay, P. L. and Freeman, S. A.: Use of optical scattering to discriminate particle types in coastal waters, Appl. Opt., 44(9), 1667, doi:10.1364/AO.44.001667, 2005.
Thomas, A. C. and Weatherbee, R. A.: Satellite-measured temporal variability of the Columbia River plume, Remote Sens. Environ., 100(2), 167–178, doi:10.1016/J.RSE.2005.10.018, 2006.
Thomson, R. E., and Fine, I. V.: Estimating Mixed Layer Depth from Oceanic Profile Data, J. Atmos. Ocean. Technol., 20(2), 319–329, doi:10.1175/1520-0426(2003)020<0319:EMLDFO>2.0.CO;2, 2003.
Thyssen, M., Grégori, G. J., Grisoni, J.-M., Pedrotti, M. L., Mousseau, L., Artigas, L. F., Marro, S., Garcia, N., Passafiume, O. and Denis, M. J.: Onset of the spring bloom in the northwestern

Mediterranean Sea: influence of environmental pulse events on the in situ hourly-scale dynamics of the phytoplankton community structure, Front. Microbiol., 5, 387, 2014.
Tortell, P. D.: Dissolved gas measurements in oceanic waters made by membrane inlet mass spectrometry, Limnol. Oceanogr. Methods, 3(1), 24–37, 2005.
Tortell, P. D., Guéguen, C., Long, M. C., Payne, C. D., Lee, P. and DiTullio, G. R.: Spatial variability and temporal dynamics of surface water pCO2, ΔO2/Ar and dimethylsulfide in the Ross Sea, Antarctica, Deep Sea Res. Part I Oceanogr. Res. Pap., 58(3), 241–259, 2011.
Tortell, P. D., Asher, E. C., Ducklow, H. W., Goldman, J. A. L., Dacey, J. W. H., Grzymski, J. J., Young, J. N., Kranz, S. A., Bernard, K. S. and Morel, F. M. M.: Metabolic balance of coastal Antarctic waters revealed by autonomous pCO2 and ΔO2/Ar measurements, Geophys. Res. Lett., 41(19), 6803–6810, 2014.
Turner, R. E., Qureshi, N., Rabalais, N. N., Dortch, Q., Justic, D., Shaw, R. F. and Cope, J.: Fluctuating silicate: nitrate ratios and coastal plankton food webs, Proc. Natl. Acad. Sci., 95(22), 13048–13051, 1998.
Twardowski, M. S., Boss, E., Macdonald, J. B., Pegau, W. S., Barnard, A. H. and Zaneveld, J. R. V.: A model for estimating bulk refractive index from the optical backscattering ratio and the implications for understanding particle composition in case I and case II waters, J. Geophys. Res. Ocean., 106(C7), 14129–14142, doi:10.1029/2000JC000404, 2001.
Waite, A. M., and Nodder, S. D.: The effect of in situ iron addition on the sinking rates and export flux of Southern Ocean diatoms, Deep Sea Res. Part II Top. Stud. Oceanogr., 48(11-12), 2635-2654, 2001.
Wanninkhof, R.: Relationship between wind speed and gas exchange over the ocean revisited, Limnol. Oceanogr. Methods, 12(6), 351–362, 2014.
Weiss, R. F. and Price, B. A.: Nitrous oxide solubility in water and seawater, Mar. Chem., 8(4), 347–359, 1980.
Westberry, T., Behrenfeld, M. J., Siegel, D. A. and Boss, E.: Carbon-based primary productivity modeling with vertically resolved photoacclimation, Global Biogeochem. Cycles, 22(2), 2008.
White, A. E., Barone, B., Letelier, R. M. and Karl, D. M.: Productivity diagnosed from the diel cycle of particulate carbon in the North Pacific Subtropical Gyre, Geophys. Res. Lett., 44(8), 3752–3760, 2017.
Wu, C.-J., Chiang, K.-P. and Liu, H.: Diel feeding pattern and prey selection of

mesozooplankton on microplankton community, J. Exp. Mar. Bio. Ecol., 390(2), 134–142, 2010.
Zeng, C., Rosengard, S. Z., Burt, W., Peña, M. A., Nemcek, N., Zeng, T., Arrigo, K. R. and Tortell, P. D.: Optically-derived estimates of phytoplankton size class and taxonomic group biomass in the Eastern Subarctic Pacific Ocean, Deep Sea Res. Part I Oceanogr. Res. Pap., 136, 107–118, 2018.

Table 1: Daily-integrated mixed layer net primary production (NPP) and net community production (NCP), including all components used to calculate NCP from $\Delta O_2/Ar$ or POC time series, as indicated: gross primary productivity (GPP), respiration (CR), vertical mixing (Mix), and gas exchange (J_{ex}). All units here are in mmol C m^{-2} d^{-1}. Note that CbPM is the Carbon-Based Production Model (Behrenfeld et al., 2005; Westberry et al., 2008; Graff et al., 2016) (Sect. 2.5).

	Drifter 1:			Drifter 2:	
	Day 1	**Day 2**	**Day 3**	**Day 1**	**Day 2**
NPP (CbPM)	147 ± 61	137 ± 51	112 ± 40	22 ± 9	18 ± 7
NPP (^{14}C)	150 ± 18	-	49 ± 8	12 ± 4	-
GPP ($\Delta O_2/Ar$)	284 ± 75	270 ± 178	358 ± 198	108 ± 101	219 ± 211
GPP (POC)	242 ± 51	106 ± 26	98 ± 35	41 ± 8	38 ± 7
R ($\Delta O_2/Ar$)	-73 ± 65	-150 ± 88	-172 ± 56	-83 ± 35	-186 ± 64
R (POC)	-77 ± 55	-147 ± 28	-104 ± 40	-44 ± 12	-36 ± 9
Mix (N_2O)	-70 ± 29	-16 ± 81	-19 ± 42	0	0
Mix (POC)	-67 ± 47	-12 ± 16	-20 ± 16	0	0
J_{ex} (daily)	-62 ± 11	-7 ± 4	-6 ± 3	12 ± 5	17 ± 7
$NCP_{O2/Ar}$	140 ± 45	104 ± 84	167 ± 52	-12 ± 44*	33 ± 20
NCP_{POC}	97 ± 49	-53 ± 24	-25 ± 31	-2 ± 3	1 ± 2

*Calculated using summed three-hour increments of $NCP_{O2/Ar}$ (refer to Table 2 and Sect. 2.6.3). All other NCP values reported here were computed using day/night linear regressions of [POC] and $[O_2]_{bio}$ against time (Sects. 2.6.1, 2.6.2).

Deleted: POC export ... [2]

Table 2: Comparisons of NCP calculated using four different time scales of integration: (rows 1-2) day/night linear regressions, (rows 3-4) summed linear regressions over 3-hour increments, (rows 5-6) the difference between two time points every 24 hours, and (rows 7-8) a single linear regression over the entire drifter period. Refer to Sect. 2.6.3 for further details. For every calculation approach, "Export + DOC" is the average difference between $NCP_{O2/Ar}$ and NCP_{POC} values ± 1 S.D. or ± the propagated error. All units here are in mmol C m^{-2} d^{-1}.

	Drifter 1:					Drifter 2:			
	Day 1	**Day 2**	**Day 3**	**Mean ± S.D.**	**Export + DOC**	**Day 1**	**Day 2**	**Mean ± S.D.**	**Export + DOC**
$NCP_{O2/Ar}$	140 ± 45	104 ± 84	167 ± 52	137 ± 32		26 ± 18	33 ± 20	29 ± 5	
NCP_{POC}	97 ± 49	-53 ± 24	-25 ± 31	7 ± 80	131 ± 79	-2 ± 3	1 ± 2	-0.8 ± 3	30 ± 2.4
$NCP_{O2/Ar}$ (3 hr)	177 ± 121	129 ± 102	122 ± 157	143 ± 30		-12 ± 44	25 ± 75	6 ± 26	
NCP_{POC} (3 hr)	119 ± 66	-86 ± 64	53 ± 140	28 ± 105	115 ± 88	-8 ± 10	-6 ± 5	-7 ± 1	14 ± 25
$NCP_{O2/Ar}$ (time points)	180 ± 54	128 ± 84	78 ± 43	129 ± 51		-4 ± 13	26 ± 11	11 ± 21	
NCP_{POC} (time points)	99 ± 48	-73 ± 21	-14 ± 19	4 ± 87	125 ± 66	-6 ± 17	-2 ± 11	-4 ± 3	15 ± 18
$NCP_{O2/Ar}$ (whole drifter trend)				103 ± 56				13 ± 9	
NCP_{POC} (drifter trend)				-21 ± 28	123 ± 62			-4 ± 2	17 ± 9

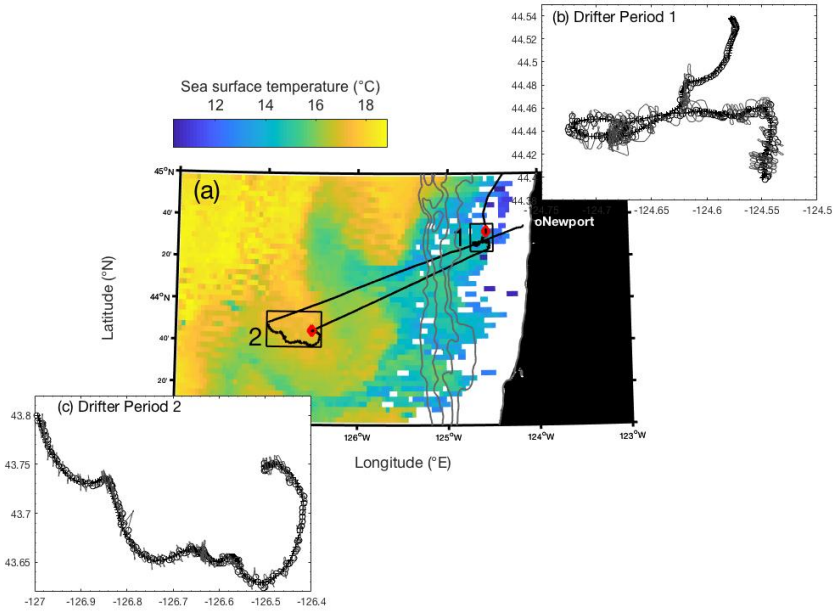

Figure 1: (a) Map of AQUA MODIS-derived 8-day composite sea surface temperature (11µm, nighttime) from 21-28 August 2017, overlapping with the duration of both drifter deployments. The two hollow boxes on the map denote location of drifter tracks, with the red diamonds indicating the location of the initial release. Gray bathymetry contours represent 0, 500, 1000, 1500 and 2000 m depths. Panels (b and c) show a detailed view of the two drifter tracks (cross symbol), with the ship's track shown in a light grey line and open circles denoting times when the ship was <1.5 km away from the drifter position. Only measurements taken at these cross-over locations were used for analysis.

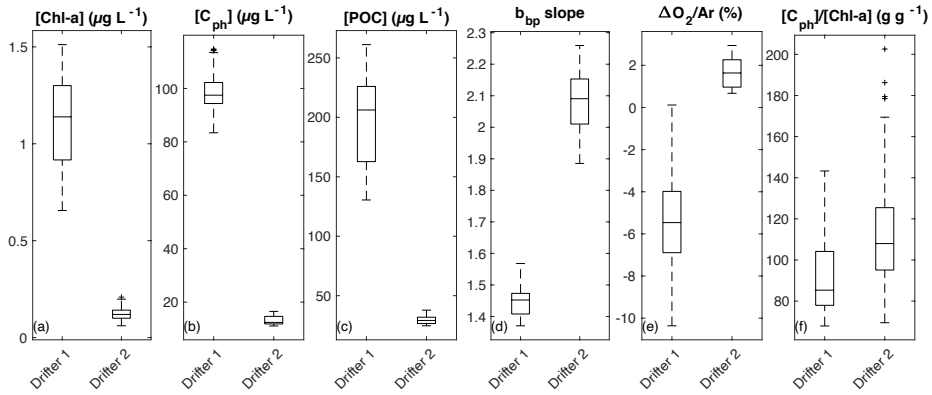

Figure 2: Comparison of average surface water properties between the two drifter deployments: (a) chlorophyll-a concentration (Chl-a), (b) phytoplankton carbon concentration (C_{ph}), (c) particulate organic carbon (POC) concentration, (d) the wavelength-dependent slope of particulate backscatter (b_{bp}), (e) biological oxygen saturation anomaly ($\Delta O_2/Ar$), and (f) the $[C_{ph}]/[Chl\text{-}a]$ ratio. Boxes represent the median (center line) and 25 and 75 percentiles (box edges). Outliers are indicated as black "+" marks.

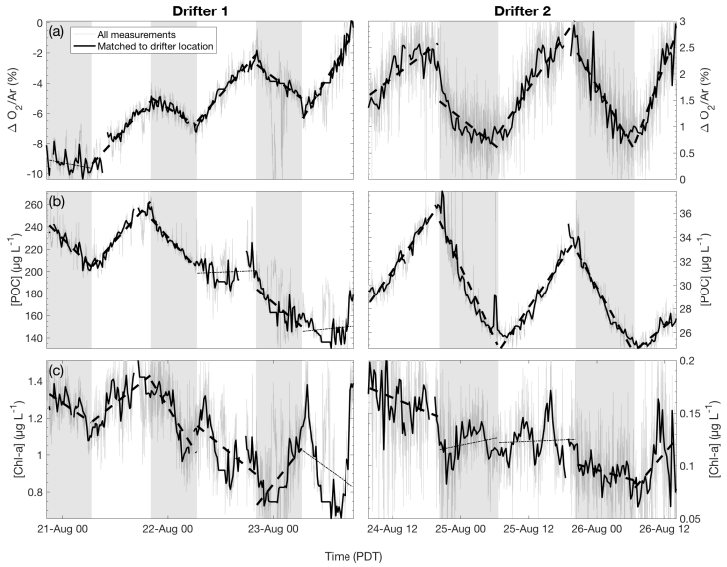

Figure 3: Time-series of (a) biological oxygen saturation ($\Delta O_2/Ar$), (b) particulate organic carbon (POC) concentration, and (c) chlorophyll-a (Chl-a) concentration during the two drifter deployments (left and right panels, respectively). For each daytime (non-shaded) and nighttime (shaded) interval, the best fit linear regression line is plotted. Significant regressions ($p<0.05$) are plotted as thick dashed lines, while non-significant regressions ($p\geq0.05$) are plotted as thin dotted lines. Grey lines show all measurements while thicker black line shows observations collected when the ship was within 1.5 km of the drifter location.

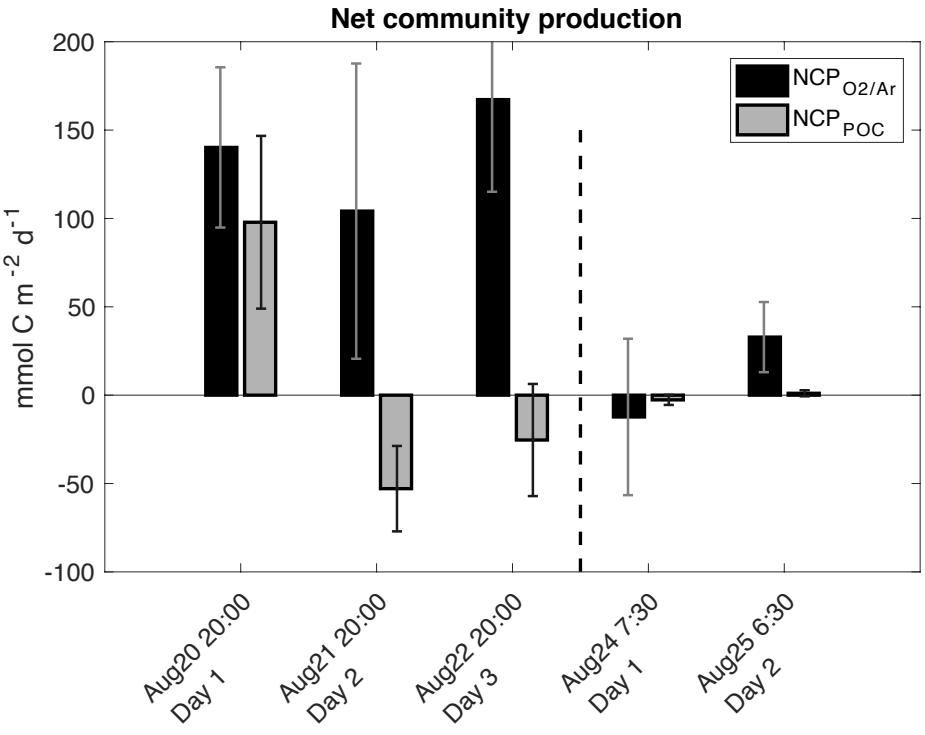

Figure 4: Daily net community production (NCP) during successive days of the two drifter deployments derived from diurnal variations of biological oxygen saturation ($\Delta O_2/Ar$) and particulate organic carbon (POC) concentration. Each set of bars is for one 24-hour period, with approximate starting times on the x-axis. Note that the negative $NCP_{O2/Ar}$ value for the first day of drifter period 2 was computed by integrating $NCP_{O2/Ar}$ values over eight consecutive three-hour increments (refer to Table 2).

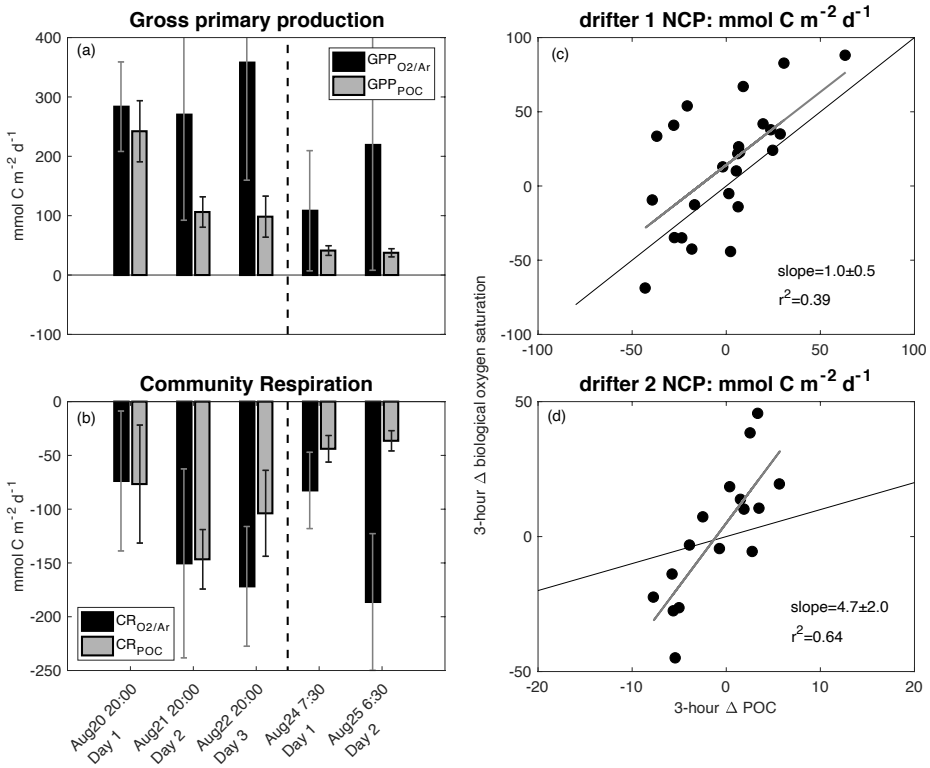

Figure 5: The left panels show comparisons between $\Delta O_2/Ar$-derived and POC-derived (a) GPP and (b) CR over the five days of both drifter deployments. The right panels show $\Delta O_2/Ar$-derived NCP ($NCP_{O2/Ar}$) as a function of POC-derived NCP (NCP_{POC}) over three-hour increments during (c) drifter period 1 and (d) drifter period 2. The vertical dashed lines in (a) and (b) indicate the break between drifter periods 1 and 2. Thin black lines in (c) and (d) represent the 1:1 line, while thicker grey lines are the best-fit from linear regressions and correspond to the indicated slope and r^2 values.

Page 36: [1] Deleted	**Microsoft Office User**	**5/5/20 3:09:00 PM**
Page 50: [2] Deleted	**Microsoft Office User**	**4/21/20 6:03:00 PM**